

Copyright
by
Siqu Wang
2016

The Thesis Committee for Siqui Wang
Certifies that this is the approved version of the following thesis:

Modeling of NORM Dosimetry
in Onshore Oilfields using Monte Carlo Methods

APPROVED BY
SUPERVISING COMMITTEE:

Supervisor:

Sheldon Landsberger

Derek Haas

**Modeling of NORM Dosimetry
in Onshore Oilfields using Monte Carlo Methods**

by

Siqiu Wang, B.S.

Thesis

Presented to the Faculty of the Graduate School of

The University of Texas at Austin

in Partial Fulfillment

of the Requirements

for the Degree of

Master of Science in Engineering

The University of Texas at Austin

December 2016

Dedication

Dedicated to my parents, Jianping Qiu and Feng Wang for the support through even the hardest times. I am truly grateful.

Acknowledgements

I would like to express my sincere gratitude to my advisor Dr. Sheldon Landsberger for the continuous support of my study and research, for his knowledge, guidance, understanding, and patience. It has been an honor to be his Masters student. I want to thank Dr. Erich Schneider for his knowledgeable inputs and my fellow graduate student Michael Yoho for his advice and support. I would also like to thank Dr. Derek Haas for being the reader on this thesis. Lastly, I am indebted to Graham George of Enviroklean Product Development Inc. (EPDI), Houston for supplying the oil scale samples to perform the radiological characterization for the input into the oilfield model.

Abstract

MCNP Modeling of NORM Dosimetry in Onshore Oilfields

Siqiu Wang, M.S.E.

The University of Texas at Austin, 2016

Supervisor: Sheldon Landsberger

NORM wastes generated in the oil and gas industry create a radioactive environment for the workers in the field. Modeling and understanding the radiation doses contributed by NORM is important in regard to radiation safety. Utilizing the Monte Carlo N-Particle code (MCNP), this work aims to provide a general estimate of the radiation dosage received by the workers. Three models are constructed to simulate the major NORM sources in an onshore oilfield: soil, scale, and sludge. A human phantom is employed to record the absorbed dose rate in each body component. The whole-body dose rate is also observed and compared with current regulations.

Table of Contents

List of Tables	viii
List of Figures	ix
Chapter 1: Introduction.....	1
1.1 Overview	1
1.2 NORM in Onshore Oilfields.....	2
1.2.1 Origin and Characteristics.....	2
1.2.2 Categorization of NORM Wastes	8
1.3 Previous Research and Objectives	15
Chapter 2 Development of the MCNP Models.....	18
2.1 Natural Soil Model as a Benchmark	20
2.2 Human Phantom.....	25
2.3 Soil	27
2.4 Scale.....	33
2.5 Sludge	36
Chapter 3 Results and Discussion.....	40
Chapter 4 Conclusion	45
Appendix A.I	46
Appendix A.II	48
Appendix A.III	56
References	57

List of Tables

Table 1:	Sample chemical composition of sludge.....	13
Table 2:	Worldwide NORM concentration in oilfield wastes	14
Table 3:	Conversion factors (nGy hr ⁻¹ per Bq kg ⁻¹) from NORM concentration in the soil to dose rate 1 m above ground	24
Table 4:	Activity concentration (Bq kg ⁻¹) of ²²⁸ Ra, ²²⁶ Ra, and ²¹⁰ Pb in the contaminated samples from a western Texas oil field	29
Table 5:	Annual dose absorption rate (mSv yr ⁻¹) in various phantom components from soil	40
Table 6:	Annual dose absorption rate (mSv yr ⁻¹) in various phantom components from pipe scale	42
Table 7:	Annual dose absorption rate (mSv yr ⁻¹) in various phantom components from separator sludge.....	43

List of Figures

Figure 1:	Radiological characteristics and relevant transport mechanisms of the ^{238}U decay series	3
Figure 2:	Radiological characteristics and relevant transport mechanisms of the ^{232}Th decay series.....	4
Figure 3:	Simplified diagram of an onshore oilfield	6
Figure 4:	Depth profile of ^{226}Ra concentration in a selected area of contaminated soil.....	10
Figure 5:	(a) Scale buildup along the pipeline (b) Oily sludge at the bottom of a tank.....	12
Figure 6:	Diagram of the benchmarking MCNP model	21
Figure 7:	Material definition for benchmark soil model	22
Figure 8:	MCNP image of the germanium detector	23
Figure 9:	Source definition for the benchmarking model	23
Figure 10:	Diagram of the ORNL phantom	26
Figure 11:	Diagram of the soil model.....	27
Figure 12:	Geometry input deck for the soil model	28
Figure 13:	Material definition for soil model.....	29
Figure 14:	Source definition for the soil model.....	30
Figure 15:	Weight window generator for the soil model	31
Figure 16:	Weight window specifications for the soil model.....	32
Figure 17:	Diagram of the scale/pipeline MCNP model	33
Figure 18:	Geometry input deck for the scale/pipeline model	34
Figure 19:	Material input deck for the scale/pipeline model.....	35

Figure 20:	Weight window specifications for the scale/pipeline model	36
Figure 21:	Simplified diagram of an oil/water separator.....	36
Figure 22:	Diagram of the sludge/separator MCNP model.....	37
Figure 23:	Geometry and material input deck for the sludge/separator model ..	38
Figure 24:	Title of Figure: (Heading 8,h8 style: TOC 8)	39

Chapter 1: Introduction

1.1 OVERVIEW

Radioactive elements of natural origin, though ubiquitous in the earth's crust and atmosphere, generally exist in relatively low concentrations and are therefore not of special health or safety concerns. However, certain industrial activities such as mining, chemical separation of minerals, oil drilling, and natural gas extraction generate by-products or wastes containing elevated levels of naturally-occurring radionuclides. These radioactive substances are known as Naturally-Occurring Radioactive Materials (NORM), or sometimes Technologically-Enhanced Naturally-Occurring Radioactive Materials (TENORM).

Some of the most common radionuclides in NORM are ^{238}U , ^{232}Th , and their progenies, many of which have half-lives on the order of billions of years. Radioactivity of these radionuclides does not diminish significantly in the time scope of human activity. Therefore, assessment of radiation exposure due to accumulation of NORM in work environments is essential for the purpose of radiation protection of personnel in the field.

The oil and gas industry deals with significant amount of NORM and employs a large work force. Oil and gas workers are at risk for a considerable amount of radiation exposure from their work environment (IAEA, 2003). For the purpose of radiation protection, this project presents a MCNP (Monte Carlo N-Particle code) simulation model for a general estimation of external, mainly gamma, radiation dose received by oil and gas workers in onshore oilfields. While internal exposure from ingestion and inhalation of NORM contaminated substances is not negligible, it is highly dependent on assigned work duties and habits of the specific individual, making its quantification challenging (Lipsztein et al., 2003). External exposure, on the other hand, is directly

related to the concentration and distribution of NORM and the geometry of the site, a MCNP model of which can provide us with information on the base radiation level that the workers are exposed to by simply being present in the field. The origins and categorizations of NORM in the oil and gas industry, as well as why MCNP is a suitable tool for dose estimation in the oil and gas field are discussed in detail in the following sections.

1.2 NORM IN ONSHORE OILFIELDS

Natural oil and gas are formed by thermal cracking of organic materials buried deep underground in sedimentary rocks. Since the process of formation occurs on a geological time scale in a mostly enclosed system, after billions of years, only extremely long-lived naturally-occurring radionuclides such as ^{40}K , ^{238}U , ^{232}Th , and their progenies can be found in the oil and gas deposits.

1.2.1 Origin and Characteristics

^{238}U , ^{232}Th , and their daughter products coexist in the state of secular equilibrium in an undisturbed environment. However, since distribution of these radionuclides within various geological components (in solid, liquid, or gas forms) is determined by their geochemical characteristics (Jonkers et al., 1997), secular equilibrium of the entire series is disrupted in a producing reservoir when leaching of oil and gas introduces forced liquid flow into the pores of the rocks, extracting liquids and gases to the surface, and leaving most solids behind. Figures 1 and 2 demonstrate how ^{238}U , ^{232}Th , and their daughter products can be transported.

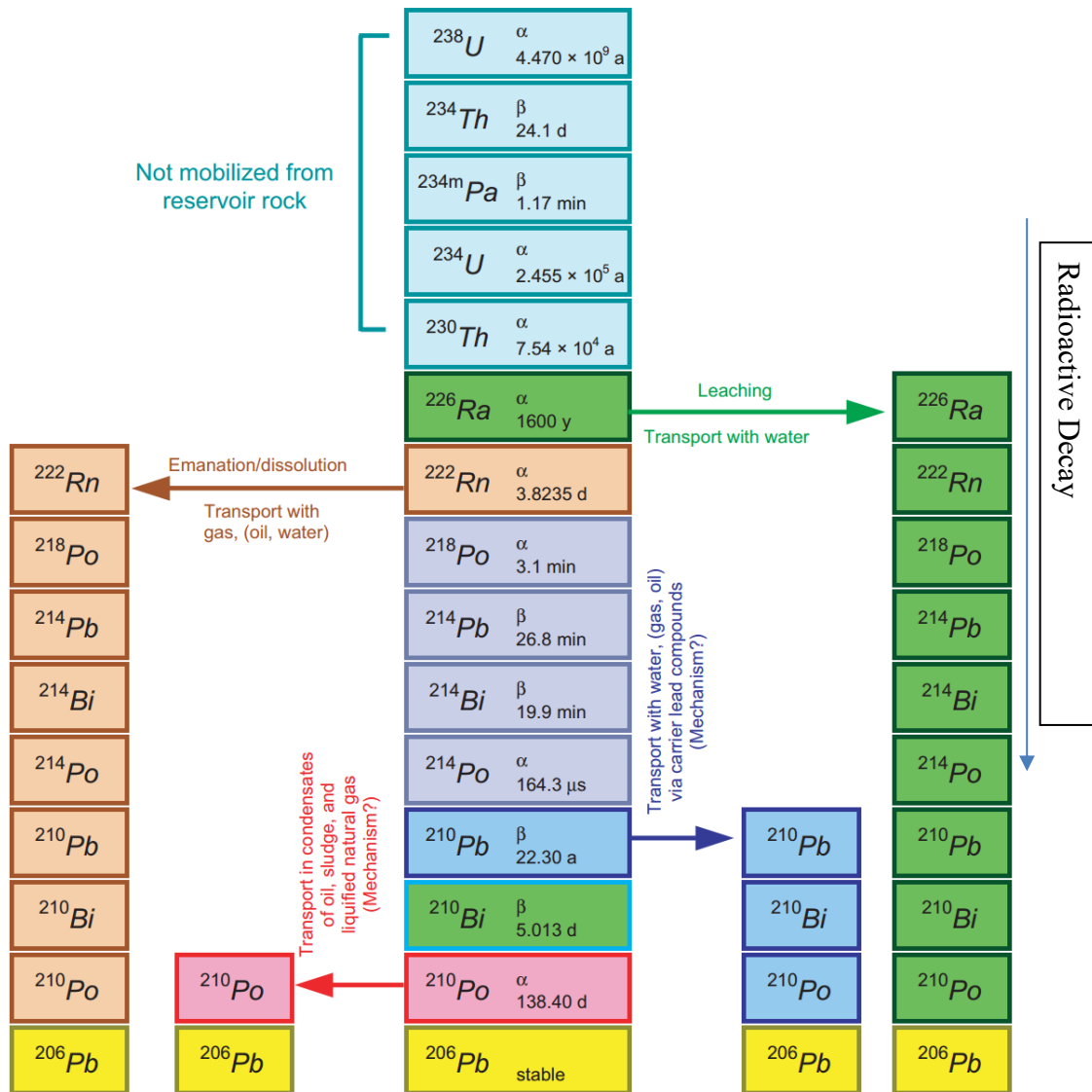


Figure 1: Radiological characteristics and relevant transport mechanisms of the ^{238}U decay series (IAEA, 2003).

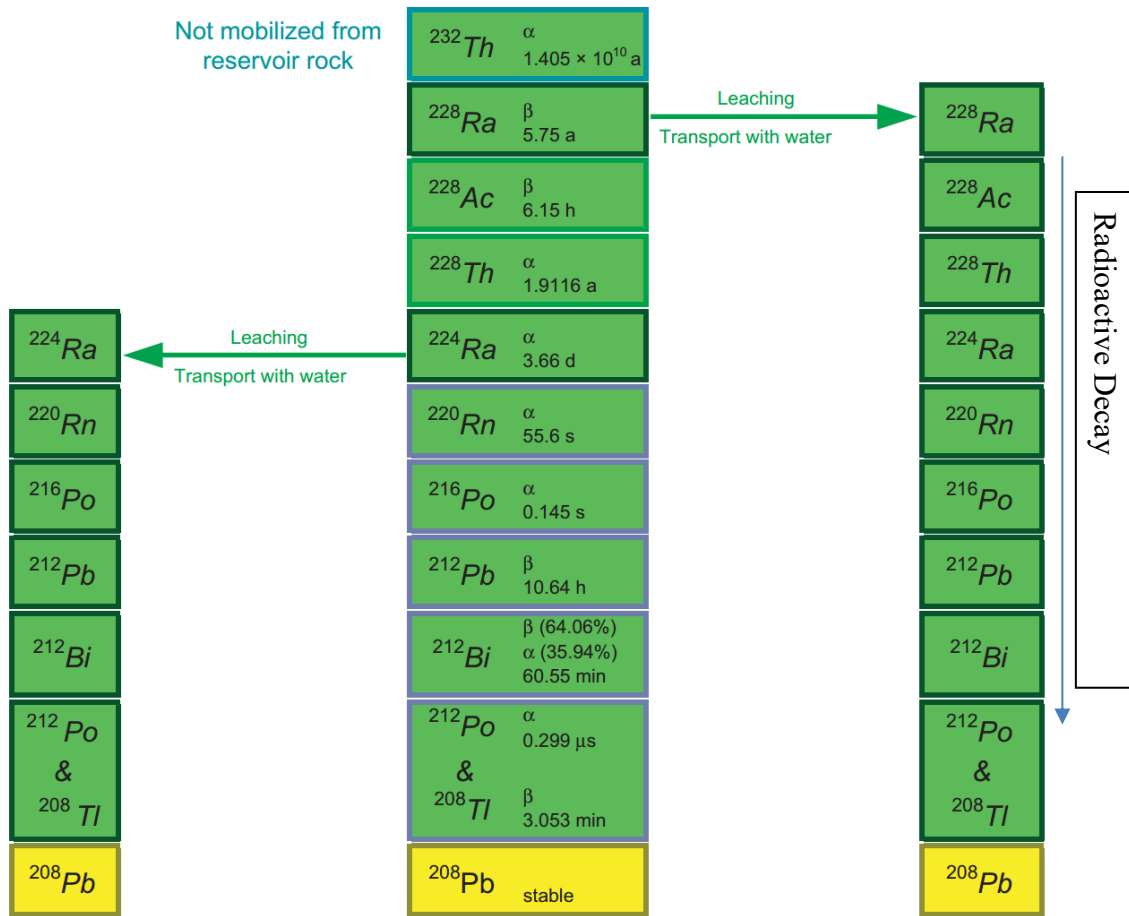


Figure 2: Radiological characteristics and relevant transport mechanisms of the ^{232}Th decay series (IAEA, 2003).

U & Th: Both uranium and thorium tend to stay in the solid phase and remain localized within the sedimentary rocks instead of being mobilized with the produced liquid/gas stream. Very rarely a small amount of uranium and thorium can be found in the form of suspended particles in the water stream. In most cases, however, they are scarcely present in above ground facilities (Jonkers et al., 1997), and are therefore not of radiological concern to the workers.

Ra: As a common daughter in both decay chains, radium is of special importance because it is water-soluble. Particularly in the reducing environment of oil reservoirs, the elevated level of salinity in water further enhances the selective leaching of radium, leading to naturally high concentrations. The radium-infused groundwater is then extracted to the surface along with crude oil and natural gas, contaminating the oil field equipment through the water stream. Essentially, NORM in the oil and gas industry are radionuclides from the partial decay chains with ^{226}Ra and ^{228}Ra as parents instead of the entire ^{238}U and ^{232}Th series.

Rn: Radon, the noble gas element, is the decay product of either ^{224}Ra or ^{226}Ra . While ^{220}Rn from the thorium series has a short half-life of 55.6 seconds and quickly decays away near where it's generated, ^{222}Rn is long-lived enough to dissipate and move around before decaying into ^{218}Po . Emanation, or escape, of radon gas from the original source materials is responsible for reduced activity of the rest of the decay chain. This phenomenon will be explored and quantified in the next section where specific categorization of NORM wastes is discussed.

Pb: In addition, an alternative transport mechanism has been suggested to be responsible for unsupported ^{210}Pb in the produced water stream (Drummond and Ohmoto, 1985; Hartog et al., 1998). However, since the process is not well understood, ^{210}Pb is sometimes individually evaluated when NORM wastes are measured.

Po: Rare occurrences of unsupported ^{210}Po in the produced water are also documented (Jonkers et al., 1997). However, neither the frequency of the events nor the recorded quantity of unsupported ^{210}Po is significant enough for separate consideration in general dose estimation.

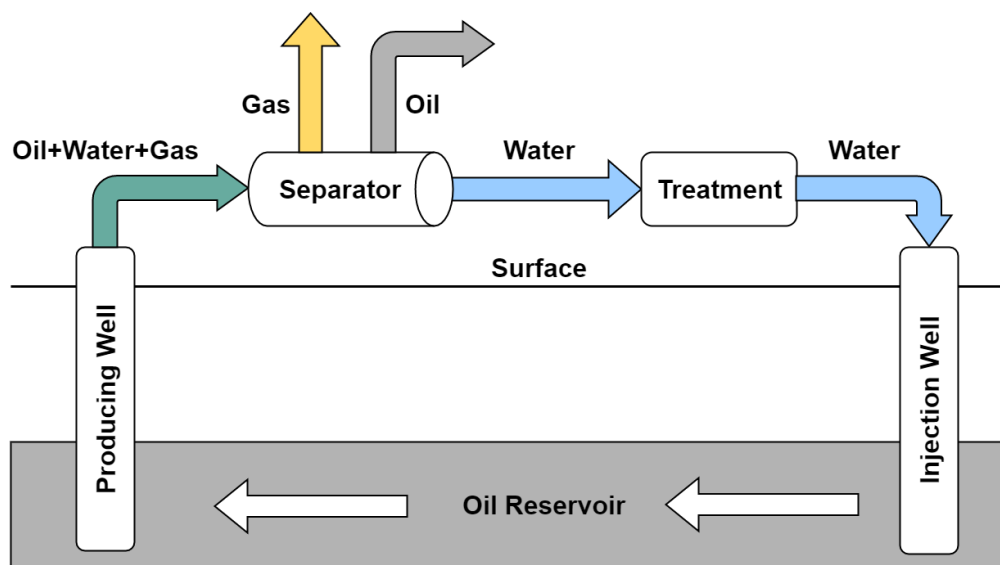


Figure 3: Simplified diagram of an onshore oilfield.

A brief examination of the oil and gas production procedure is necessary in order to understand the prevalence of each type of NORM and its relevancy to radiation dosimetry. As indicated in Figure 3. The crude oil/water/gas mixture infused with radionuclides, mainly Ra, Rn and Pb, is extracted to the surface through a producing well and transported via pipelines to the separators, where the fluids are assorted into crude oil, produced water, and natural gas, and directed toward various destinations for further processing.

Among crude oil, natural gas, and produced water, the first is the least physically or chemically capable of carrying significant amounts of naturally-occurring radionuclides. As previously discussed, radon predominantly prefers gaseous form, whereas radium and lead follow the water stream, leaving crude oil the least favorable option for NORM transportation. Correspondingly, only traces of radioactive materials have been found in crude oil and other petroleum products (Jonkers et al., 1997; Darko et al., 2011; Parmaksiz et al. 2013).

In terms of the gaseous proportion, the value of radon content in natural gas has been found to be as high as 200,000 Bq/m³ in particular cases (Jonkers et al., 1997). While inhaling ²²²Rn on a long-term basis can cause appreciable amounts of lung damage, the radioisotope itself decays by emitting weakly-penetrating alpha radiation that is unlikely to harm the workers externally. Moreover, its daughter products have a hard time amassing on the pipelines and processing equipment without water as an active chemical agent (Bjornstad and Ramsay, 1999).

Radionuclides carried by produced water turn out to be the most problematic. In response to changes in temperature, pressure, salinity, and other site conditions along the production line, radium in the water can effectively deposit and accumulate on the surface of the oil and gas field installations through co-precipitation with the other group IIA elements, such as calcium, strontium, and barium, that are abundant in well-fluids. In addition, independently transported lead ions can also be captured along the transportation path by ion exchange or electrostatic sorption reactions (Bjornstad and Ramsay, 1999). According to an investigation report from United States Geological Survey (USGS, 2011), the ²²⁶Ra and ²²⁸Ra activity concentrations found in samples of produced water from US oil and gas fields range from background to, respectively, 600 Bq/L and 100 Bq/L, which, while elevated from the natural state, do not reach an alarming level. However, with production rates typically ranging from 2,400 to 40,000 m³ per day, produced water is considered by far the largest volume of radioactive waste generated by the oil and gas industry (IAEA, 2003). Buildup of NORM wastes fed by such a large quantity of radionuclides-bearing water is certainly the main focus in terms of radiation protection.

It is worth mentioning here that in some cases, efforts have been made to prevent produced water from entering the surface facilities by using polymer gels or downhole

separators. However, such measures are not frequently adopted due to fiscal or practical limitations (Arthur et al., 2005).

1.2.2 Categorization of NORM Wastes

Deposits of NORM vary in physical appearances depending on where and how they settle. In general, NORM-contaminated wastes in the oil and gas fields can be categorized into three major forms:

1. Soil:

Soil in contact with produced water becomes contaminated with ^{226}Ra , ^{228}Ra , and ^{210}Pb through sorption, precipitation, and co-precipitation reactions (Langmuir and Melchior, 1985; Langmuir and Riese, 1985). Up until the last few decades in the United States, unregulated release of produced water in oil and gas fields had been the main source of concentrated NORM in soil. The practice, as a matter of fact, is still very much alive in other parts of the world. In the Syrian oil industry, the volume of produced water-contaminated soil that contains specific activities of ^{226}Ra more than 150 Bq/kg has been estimated to be over 100,000 m³ (Othman and Al-Masri, 2004). In the United States, direct on-site discharge of produced water is mostly prohibited at onshore production sites, with a few exceptions in areas with low-salinity water, and replaced overwhelmingly by re-injection into the isolated underground aquifers (ANL, 2009). However, most operating oilfields in the world, including many in the US (Pardue and Guo, 1997; Long et al., 2015), use unlined evaporation lagoons and waste pits as temporary storage for untreated produced water, drilling wastes, oil sludge, and etc. Consequently, as the liquids migrate underground, radioactive substances are deposited in the

surrounding soil. In addition, drilling spills, pipeline leaks, machinery failures, and other mishaps due to the highly-pressurized and corrosive nature of the transported fluids, as well as NORM wastes removal operations from pipelines and tanks also contribute to elevate radium and lead concentrations in the soil.

Activity concentration of NORM in contaminated soil varies considerably across oilfields as a result of the large selection of contamination pathways available as well as the many variables related to each pathway. Reports on the activity concentration of ^{226}Ra ranges from slightly above background, around 200 Bq/kg, in several Qatar oilfields (Al-Kinani et al., 2015) to 65,000 Bq/kg in western Texas (Landsberger et al., 2012) and 7,000- 90,000 Bq/kg across Syria (Othman and Al-Masri, 2002).

Since produced water permeates the soil from the top down, contamination is found to be concentrated at the surface layer. A study of Syrian oilfields suggests that the concentration of the main contaminant ^{226}Ra in soil declines in a logarithmic fashion as the depth increases (Figure 4) (Othman and Al-Masri, 2002). In the United States, enacted and proposed NORM-related regulations set the standard depth taken into consideration for radioactivity evaluation to 15 cm (Smith, 1992). Ideally, the computer model would simulate a 15-cm-thick layer of soil with logarithmically decreasing NORM density. However, MCNP does not provide a built-in option for logarithmically-distributed sources. While the density function can be manually set to approach a log function, it is computationally taxing to do so. Therefore, in our model NORM is assumed to be uniformly distributed in a thin top soil layer, the thickness of which is roughly estimated to be 5 cm to also account for self-attenuation.

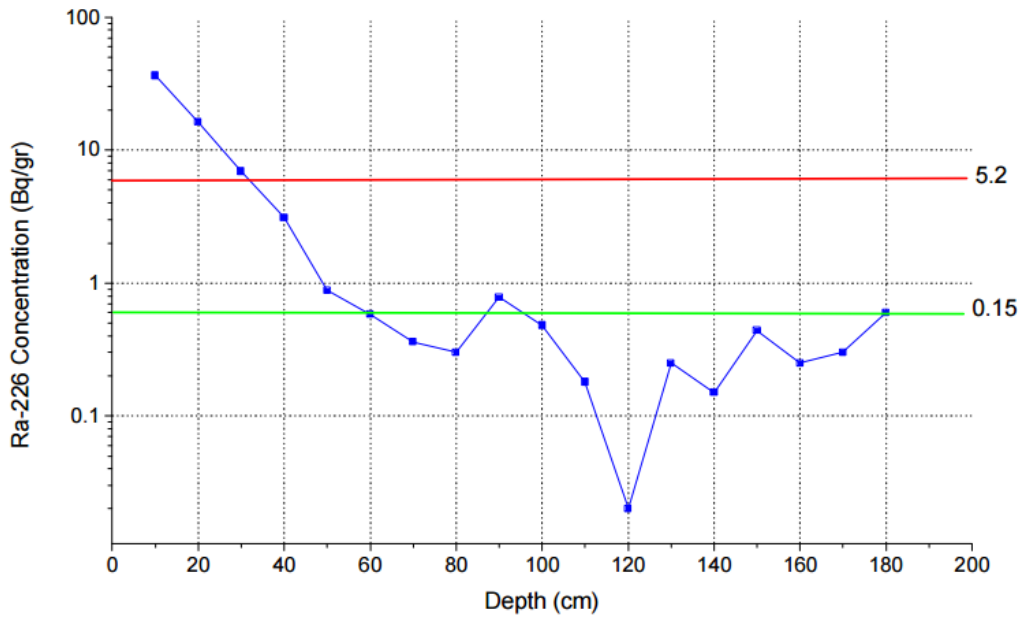


Figure 4: Depth profile of ^{226}Ra concentration in a selected area of contaminated soil.

2. Scale:

Brine, such as seawater, is commonly introduced to the oilfields to control fluid pressure in the wells. Brine is rich in sulphate and carbonate (SO_4^{2-} and CO_3^{2-}), whereas connate water from the reservoir contains abundant alkali earth ions (Ba^{2+} , Sr^{2+} and Ca^{2+}). As the two kinds of water are mixed together and transported through the production process, the solubility limits of these components can be exceeded when thermodynamic and fluid dynamic and kinetic conditions change, giving rise to the solid formation known as scale (Figure 5a) on the interior surfaces of water-handling equipment. While it is established that scale is primarily made of barium, strontium, and calcium compounds (sulfates, silicates, and carbonates) (EPA, 1991; Crabtree et al., 1999), the precise composition of these compounds varies according to geological properties and operating conditions specific to the site. An industrial standard is suggested with

the chemical formula $\text{Ba}_{0.82}\text{Sr}_{0.14}\text{Ca}_{0.028}\text{SO}_4$ and a density of 2.6 g cm^{-3} (Hamlat et al., 2003).

Radium and lead in scale exist as impurities within bulk materials and Ba, Sr and Ca lattices, making up only a small fraction of the total mass. However, activity concentration of ^{226}Ra , ^{228}Ra , and ^{210}Pb can reach a considerable level (Table 2) (IAEA, 2003), since scale is a relatively dense material. It is worth noting that the highest ^{226}Ra concentration, 15,000,000 Bq/kg, was found in samples from a Michigan oilfield.

Projections from a study in the UK suggests that the volume of scale produced in the US is estimated to be about 6,000 MT per year. Before NORM in the oil and gas industry was recognized as a radiation hazard, physical removal of scales was performed with drilling, shredding and sometimes explosions, a process known as rattling, when scale grows thick enough to impact oil production efficiency. A more modern approach is using chemical solutions to dissolve the accumulated scale. Either way, scale removal is not conducted frequently due to economic concerns. In Syrian oilfields, the average age of scales deposited in various oilfield equipment is found to be 5.3 years (Al-Masri, 2005). In the long period between removal treatments, scale can typically grow to a thickness of several inches depending on the site conditions. For this model, thickness of the scale is set to 10 cm.

Among all the interior surfaces of water-handling equipment such as control valves, pumps, storage tanks, and pipelines, NORM concentrations are found to be the highest in piping and tubing near the production well (EPA, 1991), which are therefore the main consideration in our model.

The challenge in modeling pipelines in the oilfields arises from the variety of pipes and tubes available. While pipelines are mostly consistently made of steel, their diameters range from nominal 8 in (20 cm) up to 60 in (150 cm) per ANSI/ASME Standards. Since the purpose of this project is to provide a general estimate, pipe diameter is arbitrarily set to 20 in (50 cm), which can be adjusted if more detailed analysis is needed in the future.



Figure 5: (a) Scale buildup along the pipeline. (b) Oily sludge at the bottom of a tank.

3. Sludge:

Petroleum sludge (Figure 5b) is a complex mixture of oil in water, water in oil emulsion, heavy hydrocarbons, formation sand and rocks, and other production debris. It is usually of a lower density than scale, exhibiting as a thick and viscous emulsion. Sludges typically contain high water and organic contents (30- 50% oil and 30- 50% water (Lima et al., 2014)) as well as a variety of absorptive materials (rust, sand, iron oxide, and other minerals). A sample composition of sludge is listed in Table 1.

Table 1: Sample chemical composition of sludge (Islam, 2015).

Content	Chemical composition	Weight %
Water	H ₂ O	55.13
Light hydrocarbons	C, H	23.19
Paraffin wax	C, H	10.51
Minerals and sediments	Fe, Al, Si, etc.	~10

Sludges accumulate at the bottom of storage tanks and processing vessels due to gravity and long hold-up times. To ensure production efficiency, the wastes are periodically removed and transported to offsite storage pits. Per estimation, the petroleum industry worldwide generates over 60 million tons of oily sludge every year, with more than 1 billion tons in storage pending proper disposal (Islam, 2015).

NORM radionuclides settle in sludge through precipitation, sorption, and co-precipitation with barium, strontium and calcium, much like the deposition mechanisms in scale. As shown in Table 2, while the concentration of radium is relatively lower in sludge than in scale, sludge is often found to contain unusually high quantities of unsupported ²¹⁰Pb (Jonkers et al., 1997). With ²¹⁰Pb activity concentration up to 1,300,000 Bq/kg, sludge deposited within proximity of the workers can be a considerable source of radiation.

In the oilfields, sludge is present in a dazzling range of storage and processing containers. Nevertheless, observations can be made that oil/water separators, as suggested by the name, handle the heaviest load of crude oil and produced water in the essential first step to extract petroleum and natural gas, and, as a result, host a considerable amount of

sludge. In fact, study has shown that many of the highest dose rates in the oilfield can be found next to the separators (Otto, 1989; Jonkers et al., 1997). According to specifications published by the American Petroleum Industry (API), separators are mostly cylindrical tanks with diameters ranging from 12 in (30 cm) to 60 in (150 cm) and length from 5 ft (150 cm) to 15 ft (450 cm). The model in this thesis is 35 in (90 cm) in diameter and 10 ft (300 cm) in length.

NORM activity concentrations in scale and sludge samples from around the world have been reported by IAEA, as shown below in Table 2. ^{210}Pb is measured as well as ^{226}Ra and ^{228}Ra for reasons explained in the previous section. It is evident that activity concentration of NORM varies significantly from site to site, which is a result of different geological properties (water salinity, radioactive contents in sedimentary rocks, etc.) as well as operating conditions (temperature, pressure, etc.).

Table 2: Worldwide NORM concentration in oilfield wastes (IAEA, 2003).

Radionuclide	Water (Bq L ⁻¹)	Scale (Bq kg ⁻¹)	Sludge (Bq kg ⁻¹)
^{228}Ra	0.3 - 180	50 - 2,800,000	500 - 50,000
^{226}Ra	0.02 - 1200	100 - 15,000,000	50 - 800,000
^{210}Pb	0.05 - 190	20 - 75,000	100 - 1,300,000

To evaluate the radioactive contents in the NORM wastes, it is important to understand that secular equilibrium among the entire decay chain is not applicable due to the disruption caused by the transport mechanisms and radon emanation from the source materials. The new balance established in the NORM wastes can be summarized as:

- ^{226}Ra in secular equilibrium with: ^{222}Rn
- ^{222}Rn (minus emanation rate) in secular equilibrium with:
 ^{218}Po , ^{214}Pb , ^{214}Bi , and ^{214}Po
- ^{210}Pb in secular equilibrium with: ^{210}Bi and ^{210}Po
- ^{228}Ra in secular equilibrium with all its progenies

Representative values of the emanation fraction for soil, scale, and sludge are taken into consideration since the lost radon does not locally contribute to the rest of the decay chain. Emanation rate from soil is taken to be 20% (Sakoda et al., 2011), while around 5% of radon escapes from scale. Since sludge is more granular than scale and similar to soil, radon emanation rates are around 20% as well (Nielson et al., 1998).

1.3 PREVIOUS RESEARCH AND OBJECTIVES

Since NORM wastes in the oil and gas industry began to raise concern as a potential health hazard in the 1980s, numerous surveys and investigations have been conducted to examine the potential radiation exposure caused by NORM.

The most common method is in situ dosimetry where dosimeters and detectors are either 1) placed at various locations of interests or 2) worn by the workers to record the general dosage:

- 1) An industrial-wide survey was conducted by American Petroleum Industry (API) in 1989 on a national basis to determine the difference over background in external exposure level contributed by various types of equipment (Otto, 1989). The highest exposure level found by an individual type of equipment was $44.91 \mu\text{Sv/hr}$ (4.491 mrem/hr) next to a separator. It is worth noting that

the survey treats soil as background. Moreover, since 1989, awareness has increased over NORM, and regulations have been changed. However, the survey is still relevant for the identification of equipment that are most susceptible to NORM accumulation.

A literature review of individual studies regarding radiation levels outside of various processing facilities reported up to 200 $\mu\text{Sv/hr}$ (20 mrem/hr) and 300 $\mu\text{Sv/hr}$ (30 mrem/hr) next to separators and pipelines, respectively (Jonkers et al., 1997).

- 2) A case study of the oil and gas production facilities at East Zeit Field, Egypt recorded the annual doses a group of randomly selected workers received (Eid, 1996). During a year, the maximum individual dose equivalent was reported to be 3.62 mSv (0.362 rem) while the minimum measurable value was 0.1 mSv (0.01 rem), with the average being about 1.7 mSv (0.17 rem).

Alternatively, assuming simple source geometry, several studies made dose estimations using the measured radioactivity of collected waste samples and previously-established conversion factors (Smith et al., 1995; Agbalagba et al., 2013; Parmaksiz et al., 2013). The total estimated annual effective dose ranges from 0.1 to 30 mSv (0.01 to 3 rem) depending on the site conditions and approximation methods.

The aim of this thesis is to provide an alternative method by using MCNP models to estimate the radiation dosage onshore oilfield workers received from external gamma exposure. The goal is to substitute the extensive conversion calculations required to estimate dose rates in a complex radioactive environment with a variety of radiation sources and shielding structures. Furthermore, while in situ measurement with dosimeters record the overall dose rate with a higher accuracy, the three separate models of soil, scale, and sludge provided in this thesis allow individual assessment of each source.

Furthermore, adjustments in geometry and NORM concentration can be easily implemented for further investigation. With the employment of a human phantom, dose distribution throughout the body can also be observed. It is worth pointing out that given the complexity and diversity of oilfield environments, the generalized models constructed in this project aim only to make approximations.


Chapter 2: Development of the MCNP Models

Simulations were realized with MCNP6 Version 1.0 developed by the Los Alamos National Laboratory. Monte Carlo N-Particle Transport Code, or MCNP is capable of simulating radiation transport of particles in designated media by theoretically mimicking statistical processes (Goorley et al., 2013). The code can model photons with energies from 1 keV to 100 GeV and 34 other types of particles including neutrons, electrons, light ions, and more than 2000 heavy ions over a wide range of energies. In addition, MCNP offers an extensive set of cross section libraries and physics models. Combined with its versatility in source, geometry and materials definition, MCNP provides a powerful tool for radiation-related studies.

In MCNP, each particle is generated at a source, tracked through user-defined media where it experiences numerous particle interactions, and terminated at either a tally where the desired data is recorded or a graveyard where the particle is deemed no longer important. The result of each interaction is determined by the defined physics rules and probability distributions supported by a random number generator. For each particle, this process from birth to death is called a history. Although the trajectory of one single particle seems random, as more and more histories are executed, a MCNP simulation starts to statistically resemble the real world.

To utilize the code, MCNP requires from the user an input file defining the major components of a model:

Message Block
 blank line delimiter
 One Line Problem Title Card
 Cell Cards
 blank line delimiter
 Surface Cards
 blank line delimiter
 Data Cards


Geometry

Materials
Physics
Source
Tally
Variance Reduction
 ...
 blank line terminator (optional)

As mentioned above, MCNP tracks each generated particle throughout its history. To obtain a statistically meaningful result, in many cases, on the order of 10^6 histories need to be performed, which means a large memory utilization and computation strain on the system. Therefore, the main challenge in developing a large-scale model such as an oilfield is to maximally utilize the limited time and resources and employ different model construction techniques to reduce variance and improve computational performances so that the obtained results are representative of the simulated reality.

This chapter includes the specifications of:

- 1) Benchmark
- 2) Human Phantom

- 3) Soil Model
- 4) Scale/Pipeline Model
- 5) Sludge/Separator Model

2.1 NATURAL SOIL MODEL AS A BENCHMARK

In order to ensure our capability to model large scale NORM sources, a benchmarking simulation was performed to measure the total absorbed gamma dose rate in air 1 meter above ground due to ^{40}K , ^{238}U , and ^{232}Th and their progenies in natural soil. Conversion factors (absorbed dose rate in air per unit activity per unit of soil mass, nGy h^{-1} per Bq kg^{-1}) were calculated and compared with previous studies.

The model was built after previous MCNP work (Wallace, 2013) as shown in Figure 6. The detector is placed 1 m above the disk of soil that has an even distribution of naturally-occurring radionuclides. The ^{40}K , ^{238}U decay chain, and ^{232}Th decay chain are modeled separately. The parents and daughters in the decay chains are assumed to be in secular equilibrium. Radius and depth of the soil cylinder are set to 35 m and 1 m, respectively, to simulate a semi-infinite planar source (Clouvas et al., 2000).

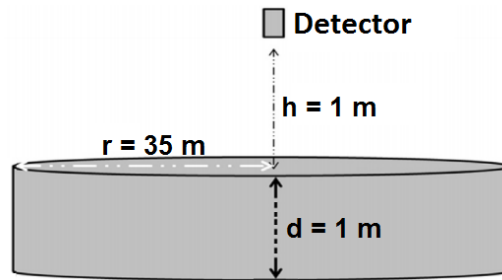


Figure 6: Diagram of the benchmarking MCNP model.

The composition of soil is taken from the standardized compendium of material composition published by Pacific Northwest National Laboratory (PNNL, 2011), compiled specifically for radiation transport modeling. Material No. 105 Earth, U.S. Average is implemented in this case. Nevertheless, variation in composition within the range of common soil has been shown to have no significant effects on the results (Gasser et al., 2014). Activity concentration of the radionuclides was arbitrarily set to 10^6 Bq kg⁻¹.

Materials in MCNP is defined as:

M[#] ZZZAAA [Atomic Fraction] ...

where ZZZ is the atomic number Z and AAA is the atomic mass number A. AAA = 000 for naturally occurring elements. Material definition of the soil is shown in Figure 7. The c symbol instructs MCNP to treat the current line as a comment and ignore it during execution. The block of text in Figure 7 defines the disk material as US average soil and ²³⁸U and its progenies which can be substituted with ⁴⁰K or the ²³²Th decay chain (commented out at the bottom).

C					
C	Earth, U.S. Average and U-238 or K-40 or Th-232				
C					
M1	8000	0.6702	11000	0.0056	\$ O and Na
	12000	0.0114	13000	0.0531	\$ Mg and Al
	14000	0.2019	19000	0.0077	\$ Si and K
	20000	0.0267	22000	0.0020	\$ Ca and Ti
	25000	0.0003	26000	0.0211	\$ Mn and Fe
	92238	7.01E-03	90234	1.04E-13	\$ U-238 and Th-234
	92234	3.85E-07	90230	1.18E-07	\$ U-234 and Th-230
	88226	2.51E-09	86222	1.64E-14	\$ Ra-226 and Rn-222
	84218	9.26E-18	82214	8.00E-17	\$ Po-218 and Pb-214
	83214	5.94E-17	84214	8.18E-24	\$ Bi-214 and Po-214
	82210	3.50E-11	83210	2.16E-14	\$ Pb-210 and Bi-210
	84210	5.95E-13			\$ Po-210
C	19040	1.97E-03			\$ K-40
C	90232	2.17E-02	88228	8.89E-12	\$ Th-232 and Ra-228
C	89228	1.09E-15	90228	2.95E-12	\$ Ac-228 and Th-228
C	88224	1.54E-14	86220	2.73E-18	\$ Ra-224 and Rn-220
C	84216	7.11E-21	82212	1.88E-15	\$ Po-216 and Pb-212
C	83212	1.78E-16	81208	8.98E-18	\$ Bi-212 and Tl-208

Figure 7: Material definition for benchmark soil model.

A germanium detector (Figure 8) was first used to monitor the quantity and energy spectrum of the absorbed photons to ensure that the source was correctly modeled. The publication describing the Ge detector used in the original work was not accessible. Therefore, the Ge detector in this benchmark model was built from scratch according to a HPGe detector at NETL. The geometry input deck is shown in Appendix A.I.

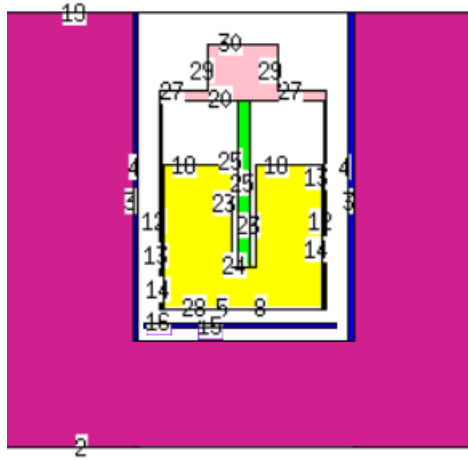


Figure 8: MCNP image of the germanium detector. The yellow region represents the germanium crystal. The magenta area represents the air outside the detector casing.

The SDEF card is used in MCNP to define the source (Figure 9). Spontaneous photon emission function PAR=sp is activated so that MCNP automatically seeks out unstable radioisotopes in the specified source cell and use photon decay data from its built-in database. The decay gammas are sampled based on the relative fractions of the radioisotopes. SI and SP cards are set so that radionuclides are evenly-distributed in the disk and emitting photons isotropically.

```
SDEF CEL=1 PAR=sp ERG=0.0 POS=0 0 -96 AXS=0 0 1 RAD=d1 EXT=d2
SI1 0 3500
SP1 0 1
SI2 0 100
SP2 0 1      $ Evenly-distributed radionuclides
ACT DG=lines
```

Figure 9: Source definition for the benchmarking model.

Previous work suggests that source and energy biasing does not significantly reduce computational burden (Wallace, 2013). Since the purpose of this model is

benchmarking, no further variance reduction techniques are employed to improve efficiency. In order to limit uncertainty to under 10% for the benchmark case, 5×10^7 histories were performed.

To measure the gamma dose rate absorbed by air, the Ge detector was replaced with an air cell. A F6 tally records the energy deposited by the absorbed photons averaged over the cell. The results, with the unit of MeV/g, are converted to absorbed dose (nGy). The time rate is derived from activity concentration of the source and the number of histories. The calculate conversion factors were compared with previous modeling works and in situ measurements (Gasser et al., 2014; Clouvas et al., 2000; Saito and Jacob, 1995; Quindos et al., 2004) as shown in Table 3.

Table 3: Conversion factors (nGy hr⁻¹ per Bq kg⁻¹) from NORM concentration in the soil to dose rate 1 m above ground.

	MCNP			In-Situ	
	Gasser	Clouvas	Saito	Quindos	This work
²³⁸ U	0.36	0.38	0.4	0.35	0.42
²³² Th	0.46	0.52	0.6	0.58	0.50
⁴⁰ K	0.035	0.039	0.042	0.043	0.045

Dose rate conversion factors derived from our benchmarking model are within agreement with previous works, with a discrepancy of less than 20% in all cases. In terms of the MCNP works, variation in results arises from multiple factors including dimensions of the soil models, specifications of the detector, as well as source energy definition. Our model utilizes the spontaneous gamma emission function in MCNP which employs an extensive library of all known photopeaks in the decay spectra. While

improving accuracy, this measure is computationally demanding. Previous works chose to only model selected photopeaks with relatively high yields.

Validation of the benchmarking model is necessary to ensure that we are simulating large-scale geometry as well as gamma emissions from NORM correctly. The oilfield soil model, in particular, is built with some of the dimensions of the benchmark to approximate an open field in the oil industry.

2.2 HUMAN PHANTOM

A human phantom is a computerized representation of the human body with geometrically approximated organs and tissues and information of their respective chemical compositions. Phantoms are often employed in radiological studies to simulate radiation effects on specific parts of human bodies. An effective human phantom needs to be representative of the human body, but at the same time not so complex that it suffers from unreasonable computation burden. The adult male human phantom built by Oak Ridge National Laboratory (ORNL) (Krstic and Nikezic, 2006) is employed to simulate the workers. The phantom is adjusted to include all major organs as shown in Figure 10.

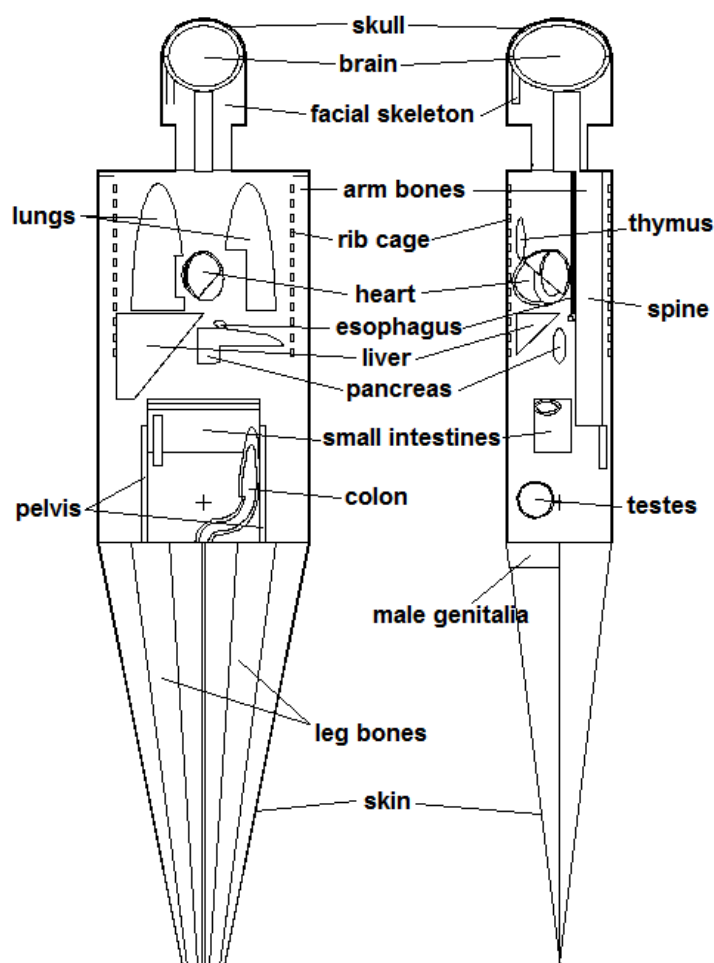


Figure 10: Diagram of the ORNL phantom.

Geometry in MCNP is constructed with cells and surfaces. Coordinates define surfaces, and surfaces define cells. The complete geometry and material input deck of the human phantom can be found in Appendix A.II.

Absorbed dose in each body part or organ is quantified individually using F6 tallies (energy deposition averaged over a cell). The collected energy data (MeV/g) are then converted to effective absorbed dose rate ($\mu\text{Sv/hr}$) as described in the benchmarking model. The complete tally deck is shown in Appendix A.III.

2.3 SOIL

Similar to the benchmarking model, soil in the oilfields is modeled as an extensive cylindrical disk (Figure 11) to simulate a semi-infinite open field. However, in this case only the top 5 cm layer is uniformly contaminated with NORM, as discussed in section 1.2.2. The radius of the disk is set to 35 m. An additional 1 m layer of normal soil is placed under the contaminated layer to account for backscattering from below. Similarly, backscattering also occurs in air, especially for photons below 100 keV. The effect, called Skyshine, is taken into consideration by expanding the air above the phantom to 10 meters. The diagram as shown in Figure 11 is not to scale.

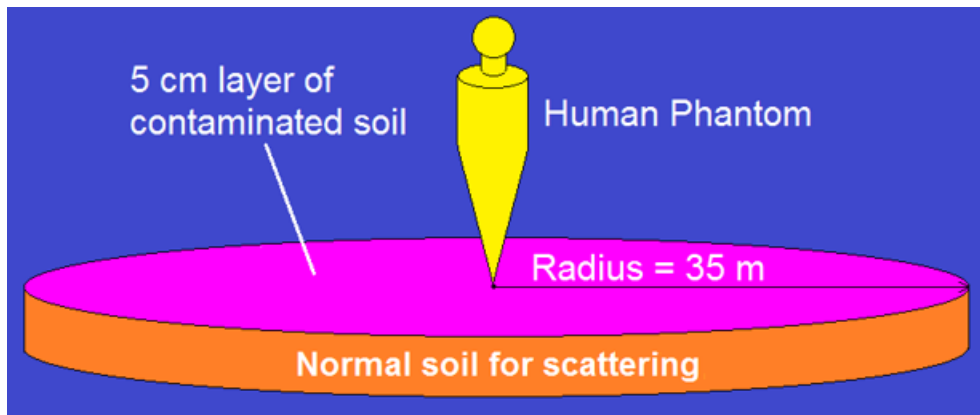


Figure 11: Diagram of the soil model.

Geometry for this soil model is relatively straightforward. The cell and surface cards are shown in Figure 12.

```

c Oilfield Soil Geometry Input Deck
c
c Cell Cards
c
c # mat mat_rho surface_definitions importance comments
1 1 -0.52 -1 3 imp:p=1 $ NORM contaminated soil
2 7 -0.52 -1 -3 imp:p=1 $ natural soil
5 2 -0.00129 (((313 4 -5 413):-4): &
(11 5 -6):(21 6 -22): &
(14 22 -12):(24 12 &
-15)) 1 2 7 -8 9 -10 &
#64 #15 imp:p=1 $ skybox minus phantom
65 0 -2:-7:8:-9:10:15 imp:p=0 $ outside skybox/graveyard
c
c ...phantom cell cards...
c

c Surface Cards
c # surface_specifications comments
1 rcc 0 0 -186 0 0 105 3500 $ soil disk (NORM + natural)
3 pz -86 $ division between NORM and natural
15 pz 1100.0 $ skybox top
2 pz -186 $ skybox bottom
7 px -3501.0 $ skybox front
8 px 3501.0 $ skybox back
9 py -3501.0 $ skybox left
10 py 3501.0 $ skybox right
c
c ...phantom surface cards...
c

```

Figure 12: Geometry input deck for the soil model. Cards related to the human phantom are omitted for presentation.

Activity concentration of NORM in the soil model is arbitrarily set. To represent an average onshore oilfield, the model uses radioactivity data collected from a western Texas oilfield (Landsberger et al., 2012) (Table 4). The atomic fraction of each radionuclide in the soil is calculated accordingly, taking into consideration equilibrium status and emanation rate of radon. Material definition of the soil is shown in Figure 13.

Table 4: Activity concentration (Bq kg⁻¹) of ²²⁸Ra, ²²⁶Ra, and ²¹⁰Pb in the contaminated samples from a western Texas oil field.

Radio-nuclide	Soil (Bq/kg)	Scale (Bq/kg)	Sludge (Bq/kg)
²²⁸ Ra	22,889 ± 740	1,370 ± 74	5,148 ± 222
²²⁶ Ra	65,296 ± 3,296	2,630 ± 148	59,000 ± 300
²¹⁰ Pb	154 ± 12	565 ± 40	28,501 ± 1,493

c	Oilfield Soil			
c				
c				
M1	8000 0.6702	11000 0.0056	\$ normal soil	
	12000 0.0114	13000 0.0531		
	14000 0.2019	19000 0.0077		
	20000 0.0267	22000 0.0020		
	25000 0.0003	26000 0.0211		
	88226 1.65E-10	86222 8.65E-16	\$ Ra-226 and Rn-222	
	84218 4.87E-19	82214 4.21E-18	\$ Po-218 and Pb-214	
	83214 3.13E-18	84214 4.30E-25	\$ Bi-214 and Po-214	
	82210 5.43E-15	83210 3.34E-18	\$ Pb-210 and Bi-210	
	84210 9.23E-17		\$ Po-210	
c	88228 2.08E-13	89228 2.54E-17	\$ Ra-228 and Ac-228	
c	90228 6.92E-14	88224 3.63E-16	\$ Th-228 and Ra-224	
c	86220 6.38E-20	84216 1.66E-22	\$ Rn-220 and Po-216	
c	82212 4.39E-17	83212 4.17E-18	\$ Pb-212 and Bi-212	
c	81208 2.10E-19		\$ Tl-208	
M2	8000 0.6702	11000 0.0056	\$ normal soil for backscatter	
	12000 0.0114	13000 0.0531		
	14000 0.2019	19000 0.0077		
	20000 0.0267	22000 0.0020		
	25000 0.0003	26000 0.0211		

Figure 13: Material definition for soil model.

It is important to address that the distribution of radionuclides is not uniform throughout a production site, since areas near NORM sources such as sediment lagoons and waste sorting stations and storage sites are naturally more affected. In order to build

an effective and representative model, the assumption is made that NORM concentration in the soil surrounding an individual worker is constant, because the dimensions of oilfield installations are significantly larger compared with the area of NORM-contaminated soil contributing to the radiation dose received by the worker.

Source definition is mostly identical to that of the benchmark except that the depth of soil bearing NORM is 5 cm instead of 1 m (Figure 14).

```
SDEF CEL=1 PAR=sp ERG=0.0 POS=0 0 -86 AXS=0 0 1 RAD=d1 EXT=d2
SI1 0 3500
SP1 0 1
SI2 0 5          $ depth of soil containing photon sources
SP2 0 1
ACT DG=lines
```

Figure 14: Source definition for the soil model.

Compared with the soil cylinder, the tallies (detectors) in the human phantom are insignificant in size, which means a single photon generated at a random position within the soil body has an extremely low probability of hitting a given tally, giving rise to large variance due to small sample size. The brute force method to resolve this issue is to execute more histories (NPS card). However, several of the smallest tallies including thyroid, thymus, and scapulae still score less than 10 collisions when NPS is as high as 10^6 , which takes about 20 hours to run.

Variance reduction techniques are therefore essential to improve accuracy while maintaining reasonable calculation efficiency. One of the most effective ways to increase sampling size and thus statistical distribution is the weight windows. It is a population control methods that utilizes particle splitting, multiplying particles entering desired regions, and Russian roulette, killing off particles less likely to contribute to target tallies,

to adjust the number of samples taken in various spaces. The physics and mathematics are kept consistent through weight preservation. For instance, when a particle enters a region twice as important, or desirable, as the region it is leaving, the particle is split into two identical ones each following its own trajectory as if no change has occurred. However, if one, or both, of the split particles ends up hitting a tally, each particle contributes only half of what it originally would, its weight reduced to 0.5.

The concept is simple. However, when complex geometry is involved, manually calculating the importance map of all cells becomes nearly impossible. In such cases, MCNP supplies a weight windows generator that helps users to determine the weight, and thus the importance of each cell. The generator works backwards, collecting information from a previous run to find out which regions need the most “help” and assigning weight bounds accordingly for use in future runs. WWG card is called during an experimental run to produce weight windows (Figure 15).

```
c Weight Window Generator
c
WWG 246 2 0 j j j 0      $ target tally F246: cell 49: thymus
c WWG 126 2 0 j j j 0    $ target tally F126: cell 26: scapulae
c WWG 196 2 0 j j j 0    $ target tally F196: cell 44: thyroid
c WWG 266 2 0 j j j 0    $ target tally F256: cell 50: adrenals
```

Figure 15: Weight window generator for the soil model.

The WWG card produces a set of weight window bounds for every cell at the end of each run. The weight windows can then be plugged back into the original input file for a second run. Each iteration helps approximate the “perfect” weight windows. In our

model, four iterations were performed for the four most poorly sampled tallies. The final set of weight windows is shown in Figure 16.

wwp:p	5	3	5	0	0	0
wwe:p	1.0000E+02					
wwn1:p	1.0000E+00	2.6338E+00	7.2362E-02	2.2981E+00	3.3961E-03	
	1.3870E-01	1.6621E-03	1.5903E-03	2.1193E-03	1.1233E-03	
	4.8329E-04	1.0482E-03	4.9308E-04	3.0042E-04	7.7065E-04	
	4.5390E-04	1.5674E-04	3.7324E-03	1.5805E-03	2.1487E-02	
	2.6450E-03	1.8613E-04	7.4779E-04	3.6704E-03	6.8085E-03	
	1.5772E-03	9.9923E-04	1.2703E-03	4.5716E-05	7.9024E-04	
	3.4940E-04	3.0042E-04	5.5513E-05	1.2082E-04	3.1675E-04	
	1.4368E-04	6.7921E-04	2.5471E-04	6.1064E-04	3.7879E-04	
	4.1471E-04	2.3511E-04	3.7879E-04	3.0042E-04	3.7063E-03	
	4.4854E-02	1.6197E-03	-1.0000E+00			

Figure 16: Weight window specifications for the soil model.

Utilization of weight windows reduces the number of histories needed for a statistically significant result from 10^6 histories. All tallies passed the 10 statistical checks MCNP performs. Relative errors are less than 10%.

2.4 SCALE

Figure 17 is a coronal diagram of the phantom and a pipeline containing scale. The pipe and scale are constructed as coaxial cylinders with dimensions shown in the diagram. The phantom is positioned 1 m away from the pipeline which extends equal length into and away from the page. In order to determine the horizontal length necessary to simulate the extensive pipelines commonly seen in the oilfields, trial runs are conducted to roughly measure the absorbed dose rate in air 1 meter away from the outer surface of the pipe using an air cell and a F6 tally, the same technique as in the benchmark model. Dose rate contributed by a 15-m-long pipe is found to be around 90% of that by a 30-m-long counterpart, while the latter proves much more computationally expensive. Therefore, the pipe model is built to be 15 m-long.

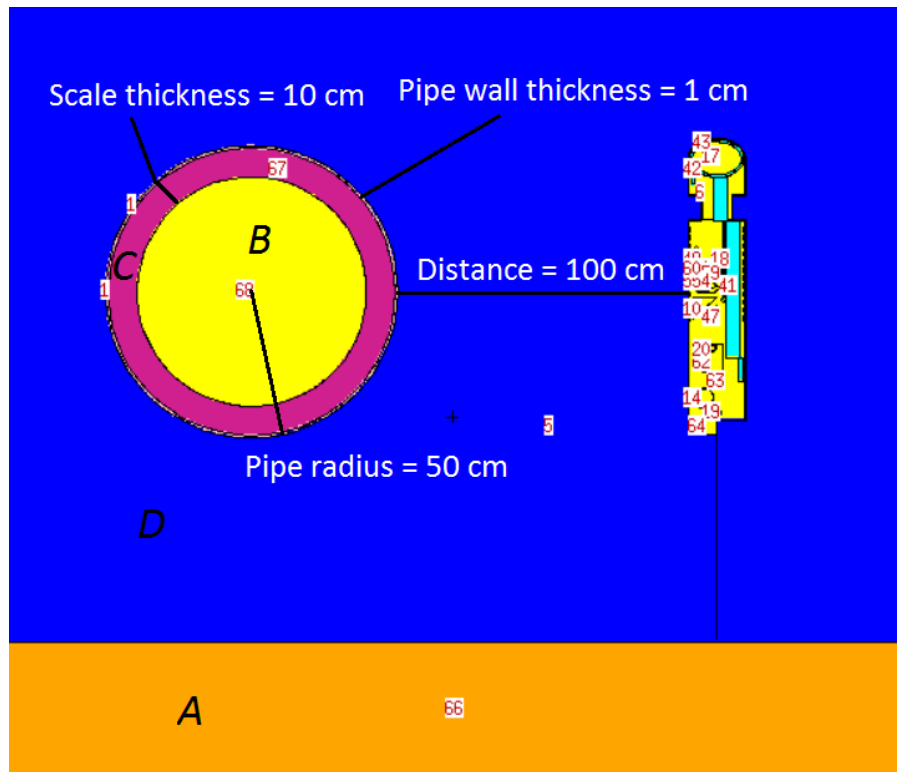


Figure 17: Diagram of the scale/pipeline MCNP model.

Other components of the model include average soil to account for backscattering (A), air (D), oil and water mixture transported by the pipeline (B), and the NORM-contaminated scale (C). It is worth noting that the diagram does not show the entire model. The air and soil extends beyond the scale of the diagram to account for Skyshine and backscatter. Geometry input deck for this model is shown in Figure 18.

```

c Oilfield Scale Geometry and Material Input Deck
c
c Cell Cards
c
c # mat mat_rho surface_definitions importance comments
  1 7  -7.82  -1 201 imp:p=1 $ pipe wall
65 0  -3:-7:8:-9:10:15 imp:p=0 $ graveyard
66 6  -1.52  -2 3 7 -8 9 -10 imp:p=1 $ normal soil
67 1  -2.6   -201 202 imp:p=1 $ NORM contaminated scale
68 3  -1.04  -202 imp:p=1 $ oil/water in the pipe
c
c ...phantom cell cards...
c

c Surface Cards
c
c # surface_specifications comments
  1 rcc -750 -200 45 1500 0 0 51 $ outer pipe wall
201 rcc -750 -200 45 1500 0 0 50 $ inner pipe wall/outer scale surface
202 rcc -750 -200 45 1500 0 0 40 $ inner scale surface
  2 pz -86 $ ground|
15 pz 600.0 $ boundary top
  3 pz -186 $ boundary bottom
  7 px -751.0 $ boundary front
  8 px 751.0 $ boundary back
  9 py -800.0 $ boundary left
10 py 500.0 $ boundary right
c
c ...phantom surface cards...
c

```

Figure 18: Geometry input deck for the scale/pipeline model.

Material definition of scale is similar to that of soil, combining the non-radioactive component $\text{Ba}_{0.82}\text{Sr}_{0.14}\text{Ca}_{0.028}\text{SO}_4$ with the NORM radionuclides. The variation in radon emanation rate, 5% instead of 20%, is also considered. The oil/water mixture carried by the pipeline is taken to be material No. 214 Oil, Crude (Light, Texas) from the compendium of material composition (PNNL 2011). Material card for the model of scale buildup in pipe is listed in Figure 19.

c Material Cards				
M1	8000 0.6680	16000 0.1670 &		\$ $\text{Ba}_{0.82}\text{Sr}_{0.14}\text{Ca}_{0.028}\text{SO}_4$
	20000 0.0047	38000 0.0234 &		
	56000 0.1369 &			
	88226 1.661E-11	86222 1.087E-16		\$ Ra-226 and Rn-222
	84218 6.122E-20	82214 5.293E-19		\$ Po-218 and Pb-214
	83214 3.930E-19	84214 5.408E-26		\$ Bi-214 and Po-214
	82210 2.315E-13	83210 1.426E-16		\$ Pb-210 and Bi-210
	84210 3.936E-15			\$ Po-210
	88228 1.177E-14	89228 1.437E-18		\$ Ra-228 and Ac-228
	90228 3.913E-15	88224 2.052E-17		\$ Th-228 and Ra-224
	86220 3.609E-21	84216 9.411E-24		\$ Rn-220 and Po-216
	82212 2.486E-18	83212 2.358E-19		\$ Pb-212 and Bi-212
	81208 1.189E-20			\$ Tl-208
M2	8000 0.6702	11000 0.0056		\$ normal soil for backscatter
	12000 0.0114	13000 0.0531		
	14000 0.2019	19000 0.0077		
	20000 0.0267	22000 0.0020		
	25000 0.0003	26000 0.0211		
M7	6000 0.0228	26000 0.9772		\$ steel,carbon
M8	1000 0.6294	6000 0.3652		\$ oil, crude (light, Texas)
	7000 0.0026	16000 0.0028		

Figure 19: Material input deck for the scale/pipeline model.

Similar with the soil model, variance reduction for the pipes also primarily employs weight windows to increase the sampling size for tallies. The generated weight windows are listed in Figure 20.

wwp:p	5	3	5	0	0	0
wwe:p	1.0000E+02					
wnn1:p	1.7562E+00	2.7152E-03	1.1384E+00	8.4486E-04	1.1296E-02	
	3.6872E-04	4.5672E-04	3.8216E-04	2.9578E-04	1.1822E-04	
	1.5520E-04	6.3183E-05	3.3125E-05	1.8570E-04	6.0785E-05	
	2.0076E-05	6.5335E-04	2.6801E-04	7.6037E-04	3.4263E-04	
	6.1231E-05	1.7689E-04	5.3870E-04	1.5765E-03	2.0661E-04	
	2.5162E-04	3.2121E-04	1.8235E-05	1.2045E-04	7.3611E-05	
	1.2492E-04	4.5282E-05	1.9407E-05	1.1443E-04	5.0859E-05	
	1.7616E-04	5.9725E-05	2.0399E-04	8.9114E-05	5.3089E-05	
	2.1414E-05	9.2795E-05	5.2197E-05	6.0830E-04	8.5417E-03	
	1.6981E-04	2.9105E-01	1.0108E+00	1.4382E+00	-1.0000E+00	

Figure 20: Weight window specifications for the scale/pipeline model.

Like the soil model, 10^6 histories were run for this model and all tallies passed the 10 statistical checks with relative error less than 10%.

2.5 SLUDGE

The separator model is built with dimensions shown in Figure 21. It is worth noting that separators are complex instruments. Our model is evidently a greatly simplified version with details omitted.

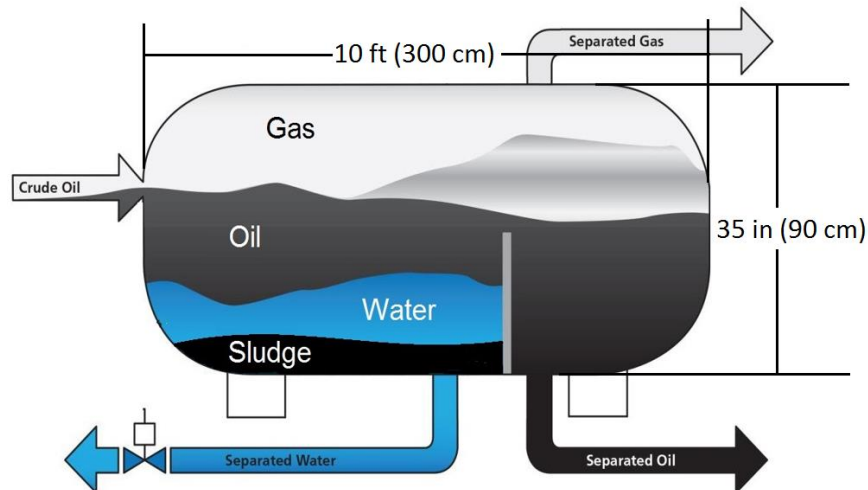


Figure 21: Simplified diagram of an oil/water separator.

The human phantom is placed 1 m away from the surface of the separator as shown in Figure 22. Contents in the separator are layers of natural gas (A), oil/water mixture (B), and sludge (C). Bottom soil is added for backscattering effect.

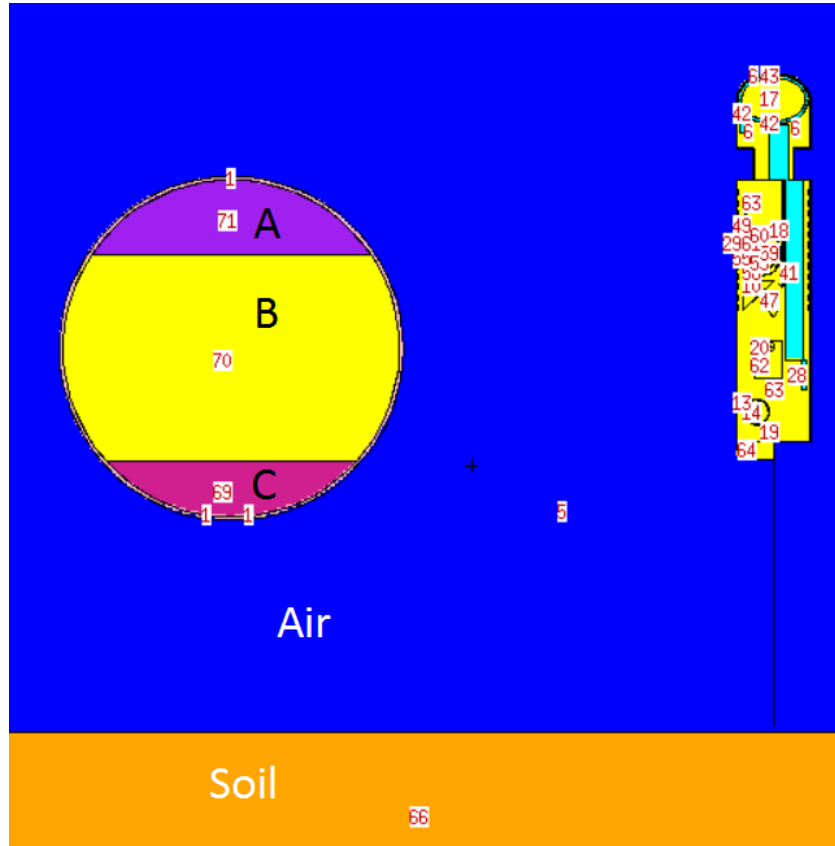


Figure 22: Diagram of the sludge/separator MCNP model.

Geometry and materials for the sludge/separator model are listed in Figure 23.

```

c Oilfield Sludge Geometry and Material Input Deck
c
c Cell Cards
c
c # mat mat_rho   surface_definitions   importance comments
  1 7   -7.82     -1 201                 imp:p=1    $ separator wall
69 1   -0.923    -201 -203                imp:p=1    $ sludge
70 3   -0.875    -201 203 -204            imp:p=1    $ oil/water mixture
71 8   -0.000667 -201 204                 imp:p=1    $ natural gas/methane
c
c ...phantom cell cards...

c Surface Cards
c
c # surface_specifications   comments
  1 rcc -750 -145 25 1500 0 0 46    $ outer surface of separator
201 rcc -750 -145 25 1500 0 0 45    $ inner surface of separator
203 pz -5                          $ oil/water and sludge interface
204 pz 50                          $ gas and oil/water interface
c
c ...phantom surface cards...

c Material Cards
M1 1000 5.026E-01 6000 2.863E-01      $ sludge (without NORM)
    7000 7.907E-04 8000 2.087E-01
    13000 3.958E-04 15000 2.678E-04
    26000 9.420E-04
    88226 4.581E-12 86222 2.399E-17    $ Ra-226 and Rn-222
    84218 1.351E-20 82214 1.168E-19    $ Po-218 and Pb-214
    83214 8.672E-20 84214 1.193E-26    $ Bi-214 and Po-214
    82210 3.535E-13 83210 2.177E-16    $ Pb-210 and Bi-210
    84210 6.011E-15                                $ Po-210
    88228 1.887E-13 89228 2.304E-17    $ Ra-228 and Ac-228
    90228 6.274E-14 88224 3.290E-16    $ Th-228 and Ra-224
    86220 5.785E-20 84216 1.509E-22    $ Rn-220 and Po-216
    82212 3.986E-17 83212 3.780E-18    $ Pb-212 and Bi-212
    81208 1.906E-19                                $ Tl-208
M9 1000 0.8 6000 0.2                $ natural gas/methane

```

Figure 23: Geometry and material input deck for the sludge/separator model.

Compared with the soil and scale/pipe models, the dimensions of the sludge/separator model are relatively manageable. Although a 10 m by 10 m air box is still in place to account for Skyshine effect, the sludge is of a much more concentrated

volume, which means a larger portion of photons are generated closer to the phantom and less likely to get lost. With the application of weight windows (Figure 24), only 5×10^5 histories are needed for meaningful results.

wwp:p	5	3	5	0	0	0
wwe:p	1.0000E+02					
wn1:p	1.393E+00	7.247E-03	1.390E+00	2.056E-03	2.454E-02	
	7.394E-04	7.336E-04	1.011E-03	5.738E-04	2.407E-04	
	3.389E-04	1.560E-04	1.175E-04	4.005E-04	1.733E-04	
	5.006E-05	1.396E-03	6.277E-04	2.070E-03	1.169E-03	
	1.252E-04	2.445E-04	1.038E-03	3.065E-03	6.238E-04	
	5.314E-04	7.933E-04	3.658E-05	2.118E-04	1.367E-04	
	1.483E-04	4.236E-05	4.428E-05	1.579E-04	7.702E-05	
	3.331E-04	1.367E-04	3.235E-04	2.118E-04	1.887E-04	
	1.155E-04	1.829E-04	1.483E-04	1.427E-03	1.805E-02	
	5.507E-04	1.000E+00	1.884E+00	-1.000E+00		

Figure 24: Weight window specifications for the sludge/separator model.

Chapter 3: Results and Discussion

After each MCNP run, an output file is generated with the tally information. The F6 tally used in our models records energy deposition averaged over the designated cell with the unit of MeV g^{-1} , which is converted to mSv by

$$\begin{aligned} 1 \text{ MeV} \cdot \text{g}^{-1} &= 1.603 \times 10^{-10} \text{ J} \cdot \text{kg}^{-1} = 1.603 \times 10^{-7} \text{ mGy} \\ &= 1.603 \times 10^{-7} \text{ mSv (photon)} \end{aligned}$$

The histories (particles generated) and the activity of the source are used to calculate the physical time of the run as

$$T_{\text{physical}}(s) = \frac{\# \text{ of histories}}{\text{Activity}}$$

Dividing the first result by the second, the dose rate (mSv s^{-1}) is converted to the annual dose rate with the assumption that the workers are in the field 2000 hours per year, which is likely an overestimation. However, the converted dose rates can be more easily compared with regulations and recommended radiation limits for better understanding of the results.

Tables 5, 6, and 7 list the annual absorbed dose rate in each body part contributed by, respectively, NORM-contaminated soil, pipe scale, and separator sludge. The data were listed in alphabetical order, and the organs receiving the highest dose rates are highlighted in bold.

Table 5. Annual dose absorption rate (mSv yr⁻¹) in various phantom components from soil.

Adrenals	0.0025	Liver	0.0221	Spine	0.0185
Arm bones	0.0578	Lungs	0.0528	Spleen	0.0087
Brain	0.0102	Male Genitalia	0.0603	Stomach	0.0119
Clavicles	0.0064	Pancreas	0.0167	Testes	0.0140
Colon	0.0398	Pelvis	0.0707	Thymus	0.0030
Esophagus	0.0021	Rib Cage	0.0686	Thyroid	0.0009
Facial Skeleton	0.0313	Scapulae	0.0011	Urinary Bladder	0.0366
Gall Bladder	0.0035	Skin	3.1445		
Kidneys	0.0061	Skull-Cranium	0.0113	TOTAL	5.03
Leg bones	1.2789	Small Intestine	0.0386		

Analyzing this table shows:

- Approximately 62.5% of the dose is absorbed by the skin. It is worth noting that the skin component in the phantom is built much thicker than actual skin to account for the tissue and fat underneath. All photons entering the body must penetrate this thick layer and deposit energy, which explains the high dose rate.
- Rib cage received about 25.4% of the dosage, effectively protecting the internal organs.

- Phantom components that are closer to the ground, such as leg bones, pelvis and genitalia, acquire relatively higher dose rates, while parts at higher elevation, such as brain, skull-cranium and thyroid, are less exposed to radiation.
- The whole-body annual absorbed dose rate is 5.03 mSv yr^{-1} . For comparison, background radiation level in the United States is about 6.24 mSv yr^{-1} , which includes the medical radiation received by the whole population averaged over per capita, resulting in 3.0 mSv yr^{-1} .

Table 6. Annual dose absorption rate (mSv yr^{-1}) in various phantom components from pipe scales

Adrenals	0.00001	Liver	0.00077	Spine	0.00042
Arm bones	0.00047	Lungs	0.00056	Spleen	0.00013
Brain	0.00016	Male Genitalia	0.00029	Stomach	0.00061
Clavicles	0.00006	Pancreas	0.00044	Testes	0.00002
Colon	0.00097	<i>Pelvis</i>	<i>0.00148</i>	Thymus	0.00006
Esophagus	0.00077	<i>Rib Cage</i>	<i>0.00127</i>	Thyroid	0.00001
Facial Skeleton	0.00041	Scapulae	0.00001	Urinary Bladder	0.00048
Gall Bladder	0.00019	<i>Skin</i>	<i>0.01056</i>		
Kidneys	0.00003	Skull-Cranium	0.00007	<i>TOTAL</i>	<i>0.02</i>
<i>Leg bones</i>	<i>0.00187</i>	<i>Small Intestine</i>	<i>0.00222</i>		

Analyzing this table shows:

- The annual absorbed dose rates contributed by pipe scales are relatively insignificant, which is a result of the scale activity concentration being two orders of magnitude smaller than that of the soil and the sludge.
- Skin absorbs a major portion, about 43.5%, of the radiation.
- The distribution of dose throughout the phantom is not directional, unlike in the soil model, which corresponds to the geometry of the sources in the models.
- The whole-body dose rate is 0.02 mSv yr⁻¹.

Table 7 Annual dose absorption rate (mSv yr⁻¹) in various phantom components from separator sludge.

Adrenals	0.0019	Liver	0.0489	Spine	0.0257
<i>Arm bones</i>	0.0720	<i>Lungs</i>	0.0348	Spleen	0.0057
Brain	0.0160	Male Genitalia	0.0329	Stomach	0.0204
Clavicles	0.0095	Pancreas	0.0048	Testes	0.0108
Colon	0.0464	Pelvis	0.0442	Thymus	0.0020
Esophagus	0.0056	<i>Rib Cage</i>	0.1098	Thyroid	0.0010
Facial Skeleton	0.0467	Scapulae	0.0005	Urinary Bladder	0.0122
Gall Bladder	0.0048	<i>Skin</i>	0.7324		
Kidneys	0.0066	Skull-Cranium	0.0086	<i>TOTAL</i>	1.51
<i>Leg bones</i>	0.1174	Small Intestine	0.0470		

Analyzing this table shows:

- Although the NORM concentration used in our sludge model is comparable with that in the soil model, the sludge has a smaller volume and thus resulted in a lower dose rate.
- The dose distribution is also not clearly directional.
- The whole-body dose rate is 1.51 (mSv yr⁻¹)

Chapter 4: Conclusion

The major contributors of radioactivity in the oil field, soil, scale, and sludge, are simulated using an MCNP code. A human phantom was utilized to observe absorbed dose rates in various body parts, among which, skin was found to receive the highest dose rate. The dose distributions are also consistent with the geometric factors.

Whole body annual absorbed doses contributed by soil, scale, and sludge are found to be, respectively, 5.03 mSv, 0.02 mSv, and 1.51 mSv, all under the regulatory values. However, it is worth noting that the NORM waste samples we modeled have a moderate level of radioactivity. Workers in oilfields with heavily contaminated soil and equipment might experience radiation exposure over the allowed limits. Further validation with in situ measurements is needed with dosimeters positioned in an oil field containing similar NORM radioactivity. For a rough comparison, previous study conducted in Egyptian oilfields (Eid, 1996) found the maximum individual dose equivalent to be 3.62 mSv/yr, with an average of 1.7 mSv/yr.

This work has demonstrated that MCNP provides a useful tool in terms of estimating radiation dose distribution in the human body in a complex radioactive environment such as the oil and gas industry, especially as a method for general approximation.

Appendix A.I

Geometry, material, and tally input deck for the HPGe detector:

```

c HPGe Detector Input Deck
c
c Cell Cards
c
c # mat mat_rho surface_definitions importance comments
2 2 -0.0012 -1 #2 #(-3 -19 15) imp:p=1 $ air
3 0 1 imp:p=0 $ void outside
5 4 -2.698 -3 15 -19 #(16 -4 -19) imp:p=1 $ aluminum housing
8 4 -2.698 -12 13 8 -20 #4 #6 #7 &
#9 #10 imp:p=1 $ crystal holder
7 5 -5.323 -13 14 8 -18 #4 #6 #9 #10 imp:p=1 $ outer electrode
4 7 -1.380 -12 5 -28 imp:p=1 $ Mylar film in IR
11 8 -1.420 -12 28 -8 imp:p=1 $ Kapton layer in IR
6 5 -5.323 -14 8 -18 #(-23 24 -18) &
#9 #10 imp:p=1 $ HPGe crystal
9 0 (-23 25 24 -18):(-13 25 &
18 -20):(16 -5 -4):(-4 12 &
5 -20):(-4 20 -19) #12 imp:p=0 $ vacuum well
10 6 -8.96 -25 24 -20 imp:p=1 $ Cu_electroincs
12 9 -2.250 (-12 20 -27):(-29 20 -30) imp:p=1 $ Teflon insulator

c Surface cards
c # surface_specifications
1 box 12.9 -13.69 -33.0 23.0 0 0 0 27.38 &
0 0 0 66.0 $ air box
3 cx 3.805 $ outer R of detector housing
4 cx 3.655 $ inner R of detector housing
5 px 25.65 $ front of window electrode
8 px 25.661047 $ front of HPGe
12 cx 2.876 $ outside of crystal holder
13 cx 2.80 $ inside of crystal holder
14 cx 2.75 $ crystal diameter
15 px 25.0 $ front of aluminum housing
16 px 25.15 $ inside of aluminum housing
18 px 30.611047 $ back of HPGe
19 px 35.90 $ back of aluminum housing
20 px 32.861047 $ back of vacuum well
23 cx 0.4 $ core hole in Ge crystal
24 px 27.111047 $ front of core hole
25 cx 0.2 $ Cu electronic
27 PX 33.181047 $ back of crystal holder
28 PX 25.650847 $ back of Mylar film in IR
29 CX 1.2 $ radius of Teflon insulator

```


30 PX 34.8

\$ back of Teflon insulator

c Tally Cards

c

c F8 tallies measure energy distribution of pulses created in a detector

c

comments

F8:p 6

\$ energy spectra in Ge crystal

F18:p 6

FT18 GEB 0.00073568688 0.00085954495 0.48984239

FT38 GEB 0.00073568688 0.00085954495 0.48984239

E0 0.0 5190I 2.01

E8 0.0 5190I 2.01

E18 0.0 5190I 2.01

E28 0.0 5190I 2.01

E38 0.0 5190I 2.01

c

c Material Cards

c

M2 6000 -0.000124 7000 -0.755268 &

8000 -0.231781 18000 -0.012827

\$ dry air ICRU

M4 13000 -1

\$ aluminium

M5 32000 -1

\$ pure germanium crystal

M6 29000 -1

\$ copper electroinc

M7 1000 -0.041960 6000 -0.625016 &

8000 -0.333024

\$ Mylar film

M8 1000 -0.026362 6000 -0.691133 &

7000 -0.073270 8000 -0.209235

\$ Kapton

M9 6000 -0.240183 9000 -0.759818

\$ Teflon insulator

M10 1000 -0.041960 6000 -0.625016 &

8000 -0.333024

\$ PET

Appendix A.II

Geometry and material deck for the human phantom:

c ORNL Adult Male Phantom

c

c Cell Cards

c

c	#	mat	mat_rho	surface_definitions	importance	comments
	1	1	-1.87	-1	imp:p=1	\$ source
	4	3	-1.04	((-13 20 -5):(-213 20 -5)) #21	imp:p=1	\$ legs
	5	2	-0.0013	((313 4 -5 413):-4):(11 5 & -6):(21 6 -22):(14 22 -12): & (24 12 -15)) 1 2 7 -8 9 -10 & #64 #15	imp:p=1	\$ outside phantom
	6	3	-1.04	((-23 6 -22 114) #44 #18 & #118):(-21 22 -322 114):((322 & -12 -18 116) #41 #43 #17): & ((-524 12 116) #43 #42)	imp:p=1	\$ head and neck
	7	3	-1.04	(-5 20 -313 13):(213 -413 -5 & 20):(4 -20 -313):(4 -20 & -413):(-11 16 5 -19):(-11 19 & -6 21):(-21 23 6 -22):(22 & -322 21 -14):(-14 18 322 & -12):(12 -24 524)	imp:p=1	\$ skin
	8	4	-0.296	(-27:28:-29:30) -25 31	imp:p=1	\$ right lung
	9	4	-0.296	(33:34:32) -26 31	imp:p=1	\$ left lung
	10	3	-1.04	-35 36 -37 -38	imp:p=1	\$ liver
	11	3	-1.04	-39 40 #47	imp:p=1	\$ stomach
	12	3	-1.04	-40	imp:p=1	\$ stomach contents
	13	3	-1.04	-41 42	imp:p=1	\$ urinary bladder
	14	3	-1.04	-42	imp:p=1	\$ bladder contents
	15	3	-1.04	(-43):(-44)	imp:p=1	\$ testes
	17	3	-1.04	-45	imp:p=1	\$ brain
	18	3	-1.04	(-48 175 37 -19):(-176 177 & -178)	imp:p=1	\$ esophagus
	118	2	-0.0013	-175 37 -19	imp:p=1	\$ air in esophagus
	19	3	-1.04	(-49 50 51 -52):(-53 54 -55 & 56):(-57 58 59 -52):(-61 62 & -59 65):(-63 64 -65 5)	imp:p=1	\$ colon
	20	3	-1.04	(-50 51 -52):(-54 -55 56): & (-58 59 -52):(-62 -59 65): & (-64 -65 5)	imp:p=1	\$ colon contents
	21	5	-1.4	(-66 20 -5):(20 -5 -67)	imp:p=1	\$ leg bones
	24	5	-1.4	(-68 5 -70 -16):(-69 5 -70 -16)	imp:p=1	\$ arm bones

25	5	-1.4	(-71 272 -72 -119):(-71 -73 & -273 -119)	imp:p=1	\$ clavicles
26	5	-1.4	(75 -74 78 -79 119 80 -81): & (75 -74 78 -79 119 -76 77)	imp:p=1	\$ scapulae
28	5	-1.4	((-83 82 -86 87 5 -85):(82 & -83 87 85 -84))	imp:p=1	\$ pelvis
29	5	-1.4	((-75 89 90 -91):(-75 89 92 & -93):(-75 89 94 -95):(-75 89 & 31 -96):(-75 89 97 -98):(-75 & 89 99 -100):(-75 89 101 & -102):(-75 89 103 -104):(-75 & 89 105 -106):(-75 89 107 & -108):(-75 89 109 -110):(-75 & 89 111 -79)) #10 #24 #25 #26	imp:p=1	\$ rib cage
41	5	-1.4	(-112 84 -90):(-112 90 -19): & (19 -113 -114)	imp:p=1	\$ spine
42	5	-1.4	-116 45 -12 #18	imp:p=1	\$ skull-cranium
43	5	-1.4	(-116 45 12 #18):(118 -117 & 120 -121 -119 116)	imp:p=1	\$ facial skeleton
44	3	-1.04	(((-125 134 -122 6 -133 123 & 127):(-126 128 -122 123 -134 & 6 -133)):((-129 131 134 -122 & 123 133 -47):(-130 132 -134 & -122 123 133 -47))) (-122 123 & -23 -124 6 -47)	imp:p=1	\$ thyroid
45	3	-1.04	(-135 65):(-136 -137)	imp:p=1	\$ kidneys
47	3	-1.04	(-138 139 -65):(-138 65 140)	imp:p=1	\$ pancreas
48	3	-1.04	-141	imp:p=1	\$ spleen
49	3	-1.04	-142	imp:p=1	\$ thymus
50	3	-1.04	(-143 145):(-144 145)	imp:p=1	\$ adrenals
52	3	-1.04	(-146 147 -148):(-149 150 148 & -348)	imp:p=1	\$ gall bladder
53	3	-1.04	(-147 -148):(-150 148 -145)	imp:p=1	\$ gall contents
54	3	-1.04	-151 152 153 #56 #57	imp:p=1	\$ heart left vent
55	3	-1.04	-152 153 #56 #57	imp:p=1	\$ HLV contents
56	3	-1.04	-154 155 153 -156 151	imp:p=1	\$ right vent
57	3	-1.04	-155 153 -156 151	imp:p=1	\$ HRV contents
58	3	-1.04	(-157 158 -153 156):(-159 160 & -153 -156)	imp:p=1	\$ heart left atrium
59	3	-1.04	(-158 -153 156):(-160 -153 & -156)	imp:p=1	\$ HLA contents
60	3	-1.04	-161 162 -153 -156 159	imp:p=1	\$ right atrium
61	3	-1.04	-162 -153 -156 159	imp:p=1	\$ HRA contents

```

62 3   -1.04   ((-82 164 -165 52 -36):(-82 &
               49 164 -165 166 -52)) #19 #20   imp:p=1   $ small intestine
63 3   -1.04   ((-16 5 -19):(19 -6 -21 114)) &
               #8 #9 #10 #11 #12 #13 #14 #18 &
               #19 #20 #24 #25 #26 #28 #29 &
               #41 #45 #47 #48 #49 #50 #52 &
               #53 #54 #55 #56 #57 #58 #59 &
               #60 #61 #62 #118   imp:p=1   $ trunk
64 3   -1.04   ((171 -5)(172 -170)(-119 169) &
               (313 413)) 43 44   imp:p=1   $ male genitalia
65 0           -2:-7:8:-9:10:15   imp:p=0   $ graveyard
c End of Cell Cards

c Surface Cards
c
c # surface_specifications   comments
15 pz 200.0   $ boundary top
2 pz -300.0   $ boundary bottom
7 px -1000.0  $ boundary left
8 px 1000.0   $ boundary right
9 py -1000.0  $ boundary front
10 py 1000.0  $ boundary back
4 pz -80.0
5 pz 0.0
6 pz 70.0
11 sq 100 400 0 0 0 0 -40000 0 0 0   $ trunk skin
12 pz 91.45
13 gq 1 1 0 0 0 -0.2 -20 0 0.04 3.96   $ left leg
313 gq 1 1 0 0 0 -0.2 -20 0 0 0   $ left leg skin
213 gq 1 1 0 0 0 0.2 20 0 0.04 3.96   $ right leg
413 gq 1 1 0 0 0 0.2 20 0 0 0   $ right leg skin
14 sq 100 64 0 0 0 0 -6400 0 0 0   $ head skin
16 sq 96.04 392.04 0 0 0 0 -37651.521 0 0 0   $ trunk
18 sq 96.04 60.84 0 0 0 0 -5843.0736 0 0 0   $ head
19 pz 69.80
20 pz -79.8
21 cz 5.4
22 pz 78.40
322 pz 78.6
23 cz 5.20   $ neck
24 sq 5112.25 3271.84 6400 0 0 0 -327184 0 0 91.45
524 sq 4638.172 2938.72 5843.074 0 0 0 -282235.1 &
      0 0 91.45

```

25 sq 32400 14400 1406.25 0 0 0 -810000 -8.50 0 & 43.50	\$ right lung
26 sq 32400 14400 1406.25 0 0 0 -810000 8.50 0 43.5	\$ left lung
27 pz 46	
28 pz 54	
29 px -5.4	
30 py 1.5	
31 pz 43.5	
32 pz 55	
33 px 8.0	
34 py 1.0	
35 sq 64 272.25 0 0 0 0 -17424 0 0 0	\$ liver start
36 pz 27	
37 pz 43	
38 p 0.028571 0.022222 -0.023256 -1	\$ liver end
39 sq 576 896 144 0 0 0 -9216 8 -4 35	\$ stomach wall
40 sq 310.914543 625.988841 65.363490 0 0 0 & -3566.739812 8 -4 35	\$ stomach contents
41 sq 142.988120 293.942933 293.942933 0 0 0 & -3514.900218 0 -4.50 8	\$ urinary bladder wall
42 sq 105.646247 227.630725 227.630725 0 0 0 & -2339.687839 0 -4.50 8	\$ bladder contents
43 sq 11.9025 8.9401 3.8025 0 0 0 -20.115225 -1.30 & -8 -2.30	\$ testes left
44 sq 11.9025 8.9401 3.8025 0 0 0 -20.115225 1.30 & -8 -2.30	\$ testes right
45 sq 2445.3025 1440.2025 3221.6976 0 0 0 & -106517.3769 0 0 91.45	\$ brain
47 pz 75.0	
48 sq 0.1764 1.3689 0 0 0 0 -0.24147396 0 2.575 0	\$ esophagus
175 sq 0.0144 0.7569 0 0 0 0 -0.01089936 0 2.575 0	
176 5 cx 0.70	
177 5 px 0.10	
178 5 px 7.80	
49 sq 6.25 6.25 0 0 0 0 -39.0625 -8.50 -2.36 0	\$ colon start
50 sq 3.20947225 3.20947225 0 0 0 0 -10.300712135 & -8.5 -2.36 0	
51 pz 14.45	
52 pz 24.0	
53 sq 0 2.25 6.25 0 0 0 -14.0625 0 -2.36 25.50	
54 sq 0 0.946729 3.892729 0 0 0 -3.68539433441 0 & -2.36 25.50	
55 px 10.50	

```

56 px -10.50
57 gq 0.282933 0.220415 0.00663757 0 0.0721253 &
    -0.0288859 -4.541008 -0.628932 0.128904 &
    17.669146
58 gq 0.556917 0.395554 0.0120398 0 0.129435 &
    -0.056858 -8.938371 -1.128675 0.271613 &
    35.669768 $ colon end
59 pz 8.72
61 ty 3.0 0 8.72 5.72 1.57 1.57
62 ty 3.0 0 8.72 5.72 0.91 0.91
63 ty 3.0 0 0 3.0 1.57 1.57
64 ty 3.0 0 0 3.0 0.91 0.91
65 px 3.0
66 gq 1 1 0.00906872 0 0 -0.200501 -20 0 1.78571 87.75 $ left leg bone
67 gq 1 1 0.00906872 0 0 0.200501 20 0 1.78571 87.75 $ right leg bone
68 gq 0.510204 0.137174 0 0 0 0.010352 -19.4898 0 &
    -0.204969 185.878 $ left arm bone
69 gq 0.510204 0.137174 0 0 0 0.010352 18.0612 0 &
    0.175983 159.592 $ right arm bone
70 pz 69
71 tz 0 11.1 68.25 20 0.7883 0.7883 $ clavicles
72 p 0.89415 1 0 11.1
73 p -0.89415 1 0 11.1
272 p 7.0342 1 0 11.1
273 p 7.0342 -1 0 -11.1
75 sq 94.09 289 0 0 0 0 -27192.01 0 0 0 $ scapulae
74 sq 95.8441 289 0 0 0 0 -27698.94 0 0 0
76 p 0.25 -1 0 0
77 p 0.80 -1 0 0
78 pz 50.9
79 pz 67.3
80 p 0.25 1 0 0
81 p 0.80 1 0 0
82 sq 127.69 127.69 0 0 0 0 -16304.7361 0 -3.8 0 $ pelvis
83 sq 144 144 0 0 0 0 -20736 0 -3 0
84 pz 22
85 pz 14
86 py 5
87 py -3
c 75 88 sq 96.04 289 0 0 0 0 -27755.56 0 0 0 $ rib cage
89 sq 86.49 272.25 0 0 0 0 -23546.9025 0 0 0
90 pz 35.1
91 pz 36.5

```

```

92 pz 37.9
93 pz 39.3
94 pz 40.7
95 pz 42.1
c 31 pz 43.5
96 pz 44.9
97 pz 46.3
98 pz 47.7
99 pz 49.1
100 pz 50.5
101 pz 51.9
102 pz 53.3
103 pz 54.7
104 pz 56.1
105 pz 57.5
106 pz 58.9
107 pz 60.3
108 pz 61.7
109 pz 63.1
110 pz 64.5
111 pz 65.9
112 sq 6.25 4 0 0 0 0 -25 0 5.50 0
113 pz 84.8
114 sq 6.25 4 0 0 0 0 -25 0 1.45 0
116 sq 3991.080625 2487.515625 5076.5625 0 0 0 &
    -224498.28515625 0 0 91.45
117 sq 81 49 0 0 0 0 -3969 0 0 0
118 sq 57.76 31.36 0 0 0 0 -1811.3536 0 0 0
119 py 0.0
120 pz 82.4
121 pz 93.13
122 c/z 0 -4.0 2.2
123 c/z 0 -4.0 1.0
124 py -4
125 gq 1 1 -0.531464 -2 0 0 -8 8 78.9413 -2915.4
126 gq 1 1 -0.531464 2 0 0 8 8 78.9413 -2915.4
127 gq 1 1 -0.109807 -2 0 0 -8 8 16.3102 -589.661
128 gq 1 1 -0.109807 2 0 0 8 8 16.3102 -589.661
129 gq 1 1 -0.0590516 -2 0 0 -8 8 7.34563 -212.437
130 gq 1 1 -0.0590516 2 0 0 -8 8 7.34563 212.437
131 gq 1 1 -0.0122007 -2 0 0 -8 8 1.51769 -31.1977
132 gq 1 1 -0.0122007 2 0 0 8 8 1.51769 -31.1977
133 pz 71.25

```

```

$ skull-cranium
$ facial skeleton

```

```

$ thyroid start

```

```

$ thyroid end

```

134 px 0
135 sq 68.0625 612.5625 45.5625 0 0 0 -1378.265625 &
6.0 6.0 32.50 \$ left kidney
136 sq 68.0625 612.5625 45.5625 0 0 0 -1378.265625 &
-6.0 6.0 32.50 \$ right kidney
137 px -3
138 sq 15.6816 2787.84 368.64 0 0 0 -4014.4896 -1.0 &
0 37 \$ pancreas
139 px -1
140 pz 37
141 sq 144 441 49 0 0 0 -1764 11 3 37 \$ spleen
142 sq 10.24 36 1.44 0 0 0 -23.04 0 -7.30 57.00 \$ thymus
143 1 sq 6.25 56.25 0.5625 0 0 0 -14.0625 0 0 0 \$ left adrenal
144 2 sq 6.25 56.25 0.5625 0 0 0 -14.0625 0 0 0 \$ right adrenal
145 1 pz 0
146 3 so 2.12 \$ gall bladder start
147 3 so 2.0
148 3 pz 0
348 3 pz 8
149 3 sq 1 1 -0.05175625 0 0 0.4823 -4.4944 0 0 0
150 3 sq 1 1 -0.05175625 0 0 0.455 -4 0 0 0 \$ gall bladder end
151 4 sq 240.25 710.7556 1849 0 0 0 -17768.89 0 0 0 \$ heart start
152 4 sq 44.3556 172.6596 729.5401 0 0 0 -2363.709924 &
0 0 0
153 4 px 0
154 4 sq 1225 3624.08 1849 0 0 0 -90601 0 0 0
155 4 sq 792.9856 2621.44 1239.04 0 0 0 -50751.0784 &
0 0 0
156 4 pz 0
157 4 sq 240.25 280.2276 729 0 0 0 -7005.69 0 0 0
158 4 sq 173.1856 203.9184 574.5609 0 0 0 &
-4504.557456 0 0 0
159 4 sq 110.25 128.5956 729 0 0 0 -3214.89 0 0 0
160 4 sq 71.5716 84.2724 574.5609 0 0 0 -1861.577316 &
0 0 0
161 4 sq 1225 1428.84 729 0 0 0 -35721 0 0 0
162 4 sq 991.6201 1167.5889 574.5609 0 0 0 &
-25792.038801 0 0 0 \$ heart end
164 py -4.86
165 py 2.20
166 pz 17
171 pz -4.8 \$ male genitalia start
172 p 1 0 0.1 -10

170 p 1 0 -0.1 10
 169 p 0 1 0.1 -10 \$ male genitalia end
 c End Surface Cards

 VOL j 20800 j 5250 2890 1810 1560 1830 152 250 45.7 & \$ cell volume
 203 37.6 1370 44.7 j 372.5 360.9 2800 956 54.7 &
 202 606 694 983 618 305 19.9 288 90.7 176 20.1 &
 15.7 10.1 53.6 177 102 67.2 108 31.6 115 27.4 111 &
 1060 43090 196 j
 TR1 3.5 5.0 38 0.616 0.788 0 -0.788 0.616 0 0 0 1 \$ surface transform
 TR2 -3.5 5 38 0.616 -0.788 0 0.788 0.616 0 0 0 1
 TR3 -4.5 -3.2 30 0.9615 0 -0.2748 -0.0574 0.9779 &
 -0.2008 0.2687 0.2090 0.9403
 TR4 1 -1.8 50 0.6751 -0.4727 -0.5664 -0.4640 0.3249 &
 -0.8241 0.5736 0.8191 0
 TR5 0 2.575 42.30 0.736084 -0.604969 -0.303634 &
 0.634945 0.772557 0 0.234575 -0.192791 0.952789
 c
 c Material Cards
 c
 M2 7000 0.8 8000 0.2 \$ air
 M3 1000 10.454E-02 6000 22.663E-02 7000 2.4901E-02 &
 8000 63.525E-02 11000 0.112E-02 12000 0.013E-02 &
 14000 0.030E-02 15000 0.134E-02 16000 0.204E-02 &
 17000 0.133E-02 19000 0.208E-02 20000 0.024E-02 &
 26000 0.005E-02 30000 0.003E-02 37000 0.001E-02 &
 40000 0.001E-02 \$ soft tissue
 M4 1000 10.134E-02 6000 10.238E-02 7000 2.8665E-02 &
 8000 75.752E-02 11000 0.184E-02 12000 0.007E-02 &
 14000 0.006E-02 15000 0.080E-02 16000 0.225E-02 &
 17000 0.266E-02 19000 0.194E-02 20000 0.009E-02 &
 26000 0.037E-02 30000 0.001E-02 37000 0.001E-02 \$ lung tissue
 M5 1000 7.3371E-02 6000 25.475E-02 7000 3.0574E-02 &
 8000 47.893E-02 9000 0.0253E-02 11000 0.326E-02 &
 12000 0.112E-02 14000 0.002E-02 15000 5.095E-02 &
 16000 0.173E-02 17000 0.143E-02 19000 0.153E-02 &
 20000 10.19E-02 26000 0.008E-02 30000 0.005E-02 &
 37000 0.002E-02 38000 0.003E-02 82000 0.001E-02 \$ bone
 MODE p

Appendix A.III

Tally input cards for the human phantom:

```

c Tally Cards
c
c F6 tallies record energy deposition averaged over specified cell(s)
c
c tally#    tallied_cell(s)          comments
F6:p        8                      $ cell 8: lung
F16:p       7                      $ cell 7: skin
F26:p       10                     $ cell 10: liver
F36:p       11 12 t                $ cell 11 and 12: stomach
F46:p       13 14 t                $ cell 13 and 14: urinary bladder
F56:p       15                     $ cell 15: testes
F66:p       17                     $ cell 17: brain
F76:p       18                     $ cell 18: esophagus
F86:p       19 20 t                $ cell 19 and 20: colon
F96:p       21                     $ cell 21: leg bones
F106:p      24 t                   $ cell 24: arm bones
F116:p      25 t                   $ cell 25: clavicles
F126:p      26                     $ cell 26: scapulae
F136:p      28                     $ cell 28: pelvis
F146:p      29                     $ cell 29: rib cage
F156:p      41                     $ cell 41: spine
F166:p      42                     $ cell 42: skull-cranium
F176:p      43                     $ cell 43: facial skeleton
F186:p      (42 43)                $ cell 42 and 43: skull
F196:p      44                     $ cell 44: thyroid
F216:p      45                     $ cell 45: kidneys
F226:p      47                     $ cell 47: pancreas
F236:p      48                     $ cell 48: spleen
F246:p      49                     $ cell 49: thymus
F256:p      50                     $ cell 50: adrenals
F266:p      (52 53)                $ cell 52 and 53: gall bladder
F276:p      (54 55 56 57 58 59 60 61) $ cell 54-61: heart
F296:p      64                     $ cell 64: male genitalia

```

References

- Agbalagba EO, Avwiri GO, Chad-Umoreh YE (2012). γ -Spectroscopy measurement of natural radioactivity and assessment of radiation hazard indices in soil samples from oil fields environment of Delta State, Nigeria. *Journal of Environmental Radioactivity*. 109:64-70.
- Agbalagba EO, Avwiri GO, Ononugbo CP (2013). Evaluation of Naturally Occurring Radioactivity Materials (NORM) of soil and sediments in oil and gas wells in western Niger Delta region of Nigeria. *Environmental Earth Sciences*. 70:2613-2622.
- Al-Kinani AT, Hushari M, Alsadig IA, Al-Sulaiti H (2015). NORM in soil and sludge samples in Dukhan oil field, Qatar state. *Donnish Journal of Research in Environmental Studies*. 2(4):37-43.
- Al-Masri MS, Aba A (2005). Distribution of scales containing NORM in different oilfields equipment. *Applied Radiation and Isotopes*. 63:457-463.
- ANL (Argonne National Laboratory) (2009). Produced water volumes and management practices in the United States. ANL. ANL/EVS/R-09/1.
- API (American Petroleum Industry) (1990). Management and disposal alternatives for NORM wastes in oil production and gas plant equipment. API. RAE-8837/2-2.
- API (2000). Overview of exploration and production waste volumes and waste management practices in the United States. HERO: Health and Environmental Research Online: 2148963.
- API (2008). Specification for oil and gas separators. API. API Specification 12J.
- Arthur JD, Langhus BG, Patel C (2005). Technical summary of oil & gas produced water treatment technologies. Tulsa, OK: All Consulting, LLC.
- Bjornstad T, Ramsøy T (1999). The “invisible” radioactive scale. Institute for Energy Technology. IFE/KR/E-99/005.
- Clouvas A, Xanthos S, Antonopoulos-Domis M, Silva J (2000). Monte Carlo calculation of dose rate conversion factors for external exposure to photon emitters in soil. *Health Physics*. 78(3):295-302.
- Crabtree M, Eslinger D, Fletcher P, Miller M, Johnson A, King G (1999). Fighting scale-removal and prevention. *Oilfield Review*. 11:35-45.
- Eid AD (1996). Radiation risk from natural radioactivity in oil and gas production industry. *Proceedings of 6th Conference of Nuclear Sciences and Applications*, Cairo, Egypt: 43-50.

- Environmental Protection Agency (EPA) (1991). Waste characterization and preliminary risk assessment. EPA. ANR-459.
- Gasser E, Nachab A, Nourreddine A, Roy C, Sellam A (2014). Update of ^{40}K and ^{226}Ra and ^{232}Th series gamma-to-dose conversion factors for soil. *Journal of Environmental Radioactivity*. 138:68-71.
- Goorley JT, Fensin ML, McKinney GW, James MR, Forster RA, Pelowitz DB, et al. (2013). MCNP6 user's manual version 1.0. Los Alamos National Laboratory. LA-CP-13-00634, Rev. 0.
- Habib AS (2012). Measurement of NORM in non-uniform scale samples from Libyan oil industry using gamma spectroscopy and Monte Carlo technique (unpublished doctoral thesis). University of Surrey, Guildford, UK.
- Haddad K, Al-Masri MS, Doubal AW (2013). Determination of ^{226}Ra contamination depth in soil using the multiple photopeaks method. *Journal of Environmental Radioactivity*. 128:33-37.
- Hamlat MS, Djeflal S, Kadi H (2001). Assessment of radiation exposures from naturally occurring radioactive materials in the oil and gas industry. *Applied Radiation and Isotopes*. 55:141-146.
- Hamlat MS, Kadi H, Fellag H (2003). Precipitate containing NORM in the oil industry: modeling and laboratory experiments. *Applied Radiation and Isotopes*. 59:95-99.
- Hassan NM (2014). Radon emanation coefficient and its exhalation rate of wasted petroleum samples associated with petroleum industry in Egypt. *Journal of Radioanalytical and Nuclear Chemistry*. DOI: 10.1007/s10967-013-2718-1.
- International Atomic Energy Agency (IAEA) (2003). Radiation protection and the management of radioactive waste in the oil and gas industry. IAEA. Safety Reports Series No. 34.
- International Association of Oil & Gas Producers (IOGP) (2016). Managing naturally occurring radioactive material (NORM) in the oil and gas industry. IOGP. Report No. 412.
- Islam B (2015). Petroleum sludge, its treatment and disposal: A review. *International Journal of Chemical Sciences*. 13(4)1584-1602.
- Jonkers G, Hartog FA, Knaepen WAI (1997). Characterisation of NORM in the oil and gas production (E&P) industry. *Proceedings of International Symposium on Radiological Problems with Natural Radioactivity in the Non-Nuclear Industry*, Amsterdam, the Netherlands. pp. 47.
- Krstic D, Nikezic D (2007). Input files with ORNL-mathematical phantoms of the human body for MCNP-4B. *Computer Physics Communications*. 176:33-37.

- Landsberger S, George G, Lara R, Tamalis D, Louis-Jean J, Dayman K (2012). Analysis of naturally occurring radioactive material using neutron activation analysis and passive Compton suppression gamma-ray spectrometry. *Nucleonika*. 57(4):461-465.
- Langmuir D, Melchior D (1985). The geochemistry of Ca, Sr, Ba and Ra sulfates in some deep brines from the Palo Duro Basin, Texas. *Geochimica et Cosmochimica Acta*. 49:2423-2432.
- Langmuir D, Riese AC (1985). The thermodynamic properties of radium. *Geochimica et Cosmochimica Acta*. 49:1593-1601.
- Lima CS, Lima RO, Silva EFB, Castro KKV, Chiavone Filho O, Soares SA, et al. (2014). Analysis of petroleum oily sludge produced from oil-water separator. *Revista Virtual de Quimica*. 6(5):1160-1171.
- Lipsztein JL, Melo DR, Sousa W, Dias da Cunha KM, Azeredo AMG, Juliao L, et al. (2003). NORM workers: A challenge for internal dosimetry programmes. *Radiation Protection Dosimetry*. 105:317-320.
- Luo H, Tang D, He W, Yan Q (2012). Distribution of Radon-222 in natural gas and its origin mechanism analysis. *World Automation Congress (WAC)*, Puerto Vallarta, Mexico. pp. 1-4.
- Othman I, Al-Masri MS (2002). Characterization of NORM contaminated sites at the Syrian oilfield: Sampling, analysis and data management. *Waste Management (WM) 2002 Conference*, Tuscon, Arizona. February 24-28, 2002.
- Othman I, Al-Masri MS (2004). Disposal strategy for NORM waste generated by the Syrian oil industry. *Proceedings of an International Symposium*, Cordoba, Spain, December 13-17, 2004. pp. 423-433.
- Otto GH (1989). A national survey on naturally occurring radioactive materials (NORM) in petroleum producing and gas processing facilities. API, Dallas Texas.
- Parmaksiz A, Agus Y, Bulgurlu F, Bulur E, Yildiz C, Oncu T (2013). Activity concentrations of ²²⁴Ra, ²²⁶Ra, ²²⁸Ra and ⁴⁰K radionuclides in refinery products and the additional radiation dose originated from oil residues in Turkey. *Radiation Protection Dosimetry*. 156(4):481-488.
- Pavlenko T, Aksyonov M, German O, Friziuk M, Fedorenko E, Mikhajlenko A (2014). NORM assessment at gas and oil fields in Ukraine. *Latest Trends in Energy, Environment and Development*. ISBN:978-960-474-375-9.
- McConn Jr RJ, Gesh CJ, Pagh RT, Rucker RA, Williams III RG (2011). Compendium of material composition data for radiation transport modeling. Pacific Northwest National Laboratory. PNNL-15870 Rev. 1.

- Quindos LS, Fernandez PL, Rodenas C, Gomez-Arozamena J, Arteche J (2004). Conversion factors for external gamma dose derived from natural radionuclides in soils. *Journal of Environmental Radioactivity*. 71:139-145.
- Ramola RC, Prasad G, Prasad Y (2007). Radon emanation from soil and groundwater and surface gamma dose rate in Budhakedar, Garhwal Himalayas, India. *Indoor and Built Environment*. 16(1):83-88.
- Saito K, Jacob P (1995). Gamma ray fields in the air due to sources in the ground. *Radiation Protection Dosimetry*. 58:29-45.
- Sakoda A, Ishimori Y, Yamaoka K (2011). A comprehensive review of radon emanation measurements for mineral rock, soil, mill tailing and fly ash. *Applied Radiation and Isotopes*. 69:1422-1435.
- Smith KP (1992), An overview of naturally occurring radioactive materials (NORM) in the petroleum industry. Argonne National Laboratory (ANL). ANL/EAIS-7.
- Smith KP, Blunt DL, Williams GP, Tebes CL (1995). Radiological dose assessment related to management of naturally occurring radioactive materials generated by the petroleum industry. SPE/EPA Exploration & Production Environmental Conference, Houston, TX, March 27-29, 1995. SPE 29712.
- Snively ES (1989). Radionuclides in produced water: A literature review. API Steering Committee, Arlington, Texas, August 16, 1989.
- US Geological Survey (USGS) (2011). Radium content of oil- and gas-field produced waters in the Northern Appalachian Basin (USA): Summary and discussion of data. USGS. Scientific Investigations Report 2011-5135.
- Vavrek MC, Hunt H, Colgan III W, Vavrek DL (2004). Status of oil brine spill site remediation. In Presentation at the 11th Annual International Petroleum Environmental Conference (IPEC), Albuquerque, NM.
- Wallace JD (2013). Monte Carlo modeling of large scale NORM sources using MCNP. *Journal of Environmental Radioactivity*. 126:55-60.